Critical Heat Flux in Countercurrent Flow

by

Charles Thomas Avedisian

B.S., Tufts University
1972

Submitted in Partial Fulfillment

of the Requirements for the

Degree of Master of

Science

at the

Massachusetts Institute of

Technology

January, 1974

Signature of Author.....
Department of Mechanical Engineering
January 25, 1974

Certified by.....
Thesis Supervisor

Accepted by.....
Chairman, Departmental Committee on Graduate Students

ABSTRACT

Title of Thesis: Critical Heat Flux in Countercurrent Flow.

Name of Author: Charles Thomas Avedisian

Submitted to the Department of Mechanical Engineering on January 25, 1974 in partial fulfillment of the requirements for the degree of Master of Science.

The results of an experimental program are presented whose purpose was to determine a correlation for Critical Heat Flux (CHF) in countercurrent flow. The principle geometry examined was that of a vertical internally heated annulus with a variable outer shroud diameter. Some data was also taken for flow inside a vertical round tube. Using saturated Freon 113 at atmospheric pressure as the working fluid, the results showed that counterflow CHF could be uniquely determined by the void fraction, the void being determined from the total measured pressure drop across the test section. The effects of geometry (varying outer shroud diameter) and flow direction (upflow and counterflow) on CHF were found to be insignificant as long as CHF was correlated with the void fraction. Also, it was found that for voids less than approximately 40%, counterflow CHF was nearly independent of void and could be approximated by pool boiling from a vertical surface.

In the high void region (greater than around 80%) CHF corresponded to flooding, while for voids less than 80% burnout occured as a result of a hydrodynamic instability and was accompanied by the onset of film boiling. In the high void region, significant pressure and flow oscillations were observed indicating that void measurements were somewhat fortuitous there.

The effects of liquid velocity and flow direction on CHF are separately noted, and the limits of the counterflow region defined.

Thesis Supervisor: Peter Griffith

Title: Professor of Mechanical Engineering

ACKNOWLEDGEMENTS

The author is sincerely grateful to Professor Peter Griffith, for whom it was a privilege to work, for his consistent encouragement and advice given throughout the course of this investigation.

He also thanks Mr. J.A. Calogerro of the Engineering Projects Laboratory for advice and help given in all phases of the construction of the apparatus.

The helpful suggestions made by Richard Smith regarding the presentation of the results, and the advice given by David Plummer at various stages of the apparatus construction, are acknowledged.

Finally, the financial support provided by the Yankee Atomic Electric Company is gratefully acknowledged.

Table of Contents

Abstract.....2
Acknowledgements.....3
List of Figures.....5
Nomenclature.....6
CHAPTER I: Introduction.....7
1.1 Background of the Problem.....7
1.2 Countercurrent Flow.....7
1.3 Flooding.....10
1.4 Critical Heat Flux.....11
1.5 Work of Others.....12
1.6 Scope of Research.....16
CHAPTER II: Experimental Program.....19
2.1 Test Section Geometry.....19
2.2 Choice of Working Fluid.....21
2.3 Description of Apparatus and Flow Loop.....24
2.3.1 Test Section and Test Tank.....27
2.3.2 Instrumentation.....30
2.4 Experimental Procedures.....32
2.5 CHF Detection.....34
2.6 Reproducibility of Data.....35
CHAPTER III: Results.....37
3.1 Void Fraction and Pressure Drop.....37
3.2 Flooding.....45
3.3 Geometric Effects on Counterflow CHF.....49
3.4 Critical Heat Flux and Void Fraction.....53
CHAPTER IV: Conclusions and Recommendations.....57
4.1 Conclusions.....57
4.2 Recommendations.....59
Appendix A: Tables III and IV.....61
Appendix B: Experimental Program to Determine CHF Inside a Vertical Round Tube.....64
B.1 Explanation of Apparatus Design.....64
B.2 Experimental Procedure and Brief Discussion of Errors.....67
References.....70

List of Figures

Figure 1 - Observed Two-Phase Flow Patterns.....72

Figure 2 - Operational Regions in Two-Phase Flow.....73

Figure 3 - Velocity Flux Plane (Zuber-Findlay graph).....74

Figure 4 - Relative Magnitude of CHF in an Annulus and.....75
a Round Tube

Figure 5 - Schematic of Counterflow Loop.....76

Figure 6 - Schematic of Upflow Loop.....77

Figure 7 - Schematic of Duct Flow Loop.....78

Figure 8 - Photograph of Test Section and Entire Apparatus...79

Figure 9 - Schematic of Test Tank and Test Section.....80

Figure 10- Relation Between Pressure Drop and Void Fraction..81

Figure 11- Relation between Pool Boiling in Water and Freon..82
113 at Elevated Pressures (using eq. 21)

Figure 12- Comparison of Voids Predicted from Pressure Drop .83
Data to Voids Predicted from the Drift Flux Model.

Figure 13- Range of Data Taken in relation to Flooding.....84

Figure 14- Effect of Heater Size on CHF.....85

Figure 15- Effect of Varying Outer Shroud Diameter on CHF....86

Figure 16- Effect of Liquid Velocity on CHF.....87

Figure 17- Effect of Liquid Velocity of Void Fraction.....88

Figure 18- Variation of CHF with "in place" quality (eq. 42).89

Figure 19- Relation between Void Fraction and Counterflow....90
CHF.

Nomenclature

A - total flow area ($A_g + A_f$)
A_g - vapor flow area
A_f - liquid flow area
D_i - heater diameter
D_o - outer shroud diameter
g - acceleration of gravity (ft/sec^2)
g_c - conversion factor ($\frac{\#_m - ft}{\#_f - sec^2}$)
h_{fg} - latent heat of vaporization
H - characteristic heater dimension (eq. 41)
J_g - superficial vapor velocity (ft/sec)
J_f - superficial liquid velocity (ft/sec)
K_1, K_2, and K_3 - constants appearing in eq. 30
L - heated length
P - pressure
q - power (Btu/hr)
q'' - heat flux ($Btu/hr\text{-}ft^2$)
R - heater resistance (electrical) (ohms)
u - actual velocity (as opposed to superficial velocity) ft/sec.
u_{gj} - vapor drift velocity (eq. 13)
V - volume

Greek:

α - void fraction
σ - surface tension ($\#_f/ft$)
τ_w - wall shear stress
ρ - density
ρ_r - electrical resitivity
ϑ - kinematic viscosity

Subscripts

g - vapor
X - cross section
f - liquid
i - inlet
CHF - critical heat flux
$max\,z$ - pool boiling predicted from eq. 21
m - momentum
f - friction
w - wall

CHAPTER I

INTRODUCTION

1.1 Background of the Problem

Two phase countercurrent flow with vapor flowing up and liquid flowing down is an important condition which is likely to occur during a loss of coolant accident (LOCA). During a LOCA, an instantaneous break of a particular size occurs in the pipe which feeds the coolant to or from the pressure vessel. This results in a rapid depressurization of the reactor core, typically from around 2200psia to atmospheric pressure in matter of seconds. During this depressurization, the flow is likely to reverse several times in a matter of seconds, creating in some regions of the fuel bundle, areas where the liquid and vapor will be flowing in opposite directions - countercurrent flow (the liquid will be flowing down and the vapor flowing up). It is this possibility of countercurrent flow during flow reversal in a LOCA which determines the importance of understanding the fluid mechanics and heat transfer of this two phase flow condition.

There are other physical situations in which countercurrent flow is of importance. Among them are flow in wickless heat pipes and film cooling of vertical fuel rods.

1.2 Countercurrent Flow

Countercurrent flow is driven by buoyancy forces due to the density differences between the gas and liquid phases. A very simple example of counter flow is simply boiling off a flat plate vertically oriented in the vicinity of an unheated surface (fig.1c) with the counterflow being due to the upflow of vapor dis-

placing downward an equal weight flow of liquid. Shown in figs. 1a and 1b is countercurrent flow in a centrally heated annulus (the principle geometry examined here). Fig.1a illustrates the observed flow pattern in counterflow, while fig.1b shows the upflow pattern. It is seen that a liquid film is postulated to be present on the heated surface (difficult to see experimentally, however) as well as the unheated surface, and that the upflow of vapor occurs in the region between. In fig.1d counterflow inside a vertical tube is shown with the liquid flowing down the tube wall and the vapor up the center core (the annular flow regime). Shown also in figs.1e and 1f are the phase separation and flow directions of upflow and downflow respectively. It is seen in these illustrations that the main difference in upflow, downflow, and countercurrent flow is simply the direction in which the phases are moving. These flow configurations are related in that at certain liquid and vapor velocities, upflow, countercurrent flow, or downflow can occur.

In any two phase flow system with heat addition, the void fraction (volume of vapor divided by total volume) is of great importance because it describes how much vapor (or liquid) is present in the system. By definition,

$$\alpha = V_g/V \qquad 1.$$

For convenience in two phase flow analysis, it is customary to use what are known as "superficial" velocities (j) rather than true velocities (u). The superficial velocities of the vapor and liquid respectively are found by dividing the measured volume flow rate by the total flow area:

$$J_g = Q_g/A \qquad 2,$$

and

$$J_f = Q_f/A \qquad 3.$$

Q_g and Q_f are the vapor and liquid volume flow rates respectively assuming only vapor or liquid is flowing in the total flow area. The superficial velocities are related to the true velocities of the liquid and vapor, u_f and u_g respectively, through the void fraction as follows:

$$J_g = \alpha u_g \qquad 4$$

and

$$J_f = u_f(1-\alpha) \qquad 5.$$

The reason for using superficial velocities is that in writing continuity and momentum equations, the true areas of the vapor and liquid (A_g and A_f respectively) are unknown. Since,

$$A_g = \alpha A \qquad 6,$$

and

$$A_f = (1-\alpha)A \qquad 7,$$

knowledge of the void and the total flow areas provides a convenient base upon which calculations can be made.

The volumetric flux density, j, is defined as the vectorial sum of j_g and j_f:

$$\vec{J} = \vec{J}_g + \vec{J}_f \qquad 8.$$

The sign convention used is that the velocity is positive upward for a vertical geometry. Hence, for both phases flowing up (upflow),

$$J = J_g + J_f \qquad 9$$

(note that the quantities in eq. 9 are scalars). For both phases flowing downward,

$$J = -J_g - J_f \qquad 10$$

(downflow). And for vapor flowing up and liquid flowing down (countercurrent flow),

$$J = J_g - J_f \qquad 11.$$

It is clear from eq. 11 that the counterflow region can be defined in two ways. The first is that eq. 11 as it stands defines countercurrent flow. That is, $j_f < 0$. Then, j can be either positive or negative and still be in the counterflow region. The second definition, attributed to Zuber et. al. (2), is a further restriction on the first definition. Namely that not only must j_f be less than zero (liquid flowing down), but $|j_f|$ must be greater than $|j_g|$. Hence only those conditions which: 1) have liquid flowing down and vapor flowing up; and 2) have $|j_f| > |j_g|$ so that j in eq. 11 is negative are considered to be in countercurrent flow. This can be more easily seen by considering fig. 2 which shows the operational regions of two phase flow (reproduced from reference 2). In region I both up and counterflow can exist since eqs. 11 and 9 with $|j_g| > |j_f|$ give positive j (j_g is positive). In region II Zuber's definition of counterflow applies where $|j_f| > |j_g|$ and hence j is negative (eq. 11) while j_g is still positive. Finally in region III, the vapor flow has reversed its direction and is now flowing downward in the direction of the liquid flow (j_f is negative from the sign convention), and hence both j_g as well as j_f are negative. This is the region of downflow (eq. 10). Fig. 3 shows that all the counterflow data taken fell in region I, and that the liquid velocity was not high enough to cause j to be negative (j_g was always greater than j_f).

1.3 Flooding

Common to all countercurrent flows is that at high vapor or liquid flow rates, the surface of a liquid film becomes increas-

ingly more wavy. The interaction of the gas stream and surface waves of the falling film can result in a retardation of the film, and a condition known as flooding may result. Flooding is the point at which the pressure rises sharply in the tube (or annulus) with the slightest increase in gas velocity and the liquid begins to move in the direction of the gaas flow - flow reversal (3). Hewitt and Hall-Taylor (4) define flooding as the transition to a region in which both climbing and falling film flow are occuring simultaneously. In any case flooding is determined by both the liquid and gas velocities. At any given gas rate, there is a definite liquid rate at which the column will flood and vice-versa. Hewitt and Hall-Taylor (4) have pointed out that the interfacial shear stress exerted by the gas phase on the liquid film is usually insufficient to cause flow reversal, and that the interfacial shear does not significantly influence flooding phenomenon.

Flooding can result in either a flow reversal, liquid hold-up, or a flow regime change. In this study flooding corresponded to large pressure fluctuations in the annulus geometry, and for the limited round data taken, to a flow regime change preceeded by a very turbulent, jiggling, motion of the liquid. These large pressure fluctuations occured only at high void fractions (usually greater than 80%).

1.4 Critical Heat Flux

The critical heat flux (CHF) is defined as the maximum in the heat flux (q/A) versus temperature curve (the boiling curve). This condition can be characterized by a vapor blanket covering the heated

surface, film dryout, flooding, or any other mechanism which will prevent liquid from cooling the heated surface resulting in a large temperature excursion. Alternatively, this condition can also be called departure from nucleate boiling (DNB) since nucleate boiling usually exists on the heated surface prior to the vapor film formation. The term "burnout" is often applied to the critical condition and implies a physical destruction of the heater. Since physical burnout never actually occured in this study, CHF is the term used to describe the limiting heat flux.

Since CHF is accompanied by a rapid wall temperature excursion, information on the value of the heat flux immediately preceeding this condition is of great importance. One purpose of this study was to collect enough data to arrive at a correlation for counterflow CHF.

1.5 Work of Others

Any paper dealing with flooding phenomenon is concerned with countercurrent flow. In the literature there exists many studies on flooding (e.g., Hewitt and Hall-Taylor (4) in their flooding analysis give a good survey of the literature). Little has been written, however, on counterflow CHF or, for that matter, on heat transfer in countercurrent flow. Dukler (5) numerically solved the governing equations for a film of liquid falling down a vertical heated surface for the velocity distribution and film thickness. Schumann (6), and Griffith, Schumann and Neustal (7) studied burnout in closed end vertical tubes with the flow rates of liquid and vapor equal at the test section exit (continuity), and specifically identified their system as being in countercurrent

flow. In their study CHF was thought to be due to liquid hold-up (flooding) and an attempt was made to verify this by comparing vapor velocities measured in separate flooding experiments with vapor velocities calculated from the CHF experiments assuming equilibrium flow, i.e.,

$$j_g = q'' \cdot A_s / A_x h_{fg} \rho_g \qquad 12.$$

Schuman (6) was only able to conclude that, to an order of magnitude, the vapor velocity neccessary to cause flooding could be used to calculate the burnout heat flux using eq. 12. CHF in his experiments was due to liquid starvation arising from flooding at the mouth of the tube. It is important to point out in Schumanns study that he recognized that the motion of the two phases in opposite directions played a definite role in the burnout of vertical tubes closed at the bottom. Countercurrent flow in the experiments of Schumann occured as a result of the rising vapor at the mouth of the tube displacing downward the same weight flow of liquid. Also, his experiments were conducted inside tubes which he recognized as producing a very turbulent counterflow motion of liquid and vapor which resulted in some ambiguity in data measurements. Similar problems were also encountered in the CHF experiments conducted inside a vertical tube in this program. For the most part CHF experiments reported here occured as a result of a critical wall flux being exceeded and not a critical vapor flow rate out the mouth of the tube as in Schumann's experiments.

Shires, Pickering and Blacker (8) studied CHF in film cooling of vertical electrically heated rods enclosed in a larger diameter shroud (essentially an annulus) in which liquid hold-up

was identified as only one of a number of mechanisms which might produce CHF. Film dryout, progressive evaporation, and sputtering (the condition in which a violent disruption occurs on the boundary of a liquid film falling onto a hot surface, essentially stripping the liquid from the heated surface altogether) were found to cause burnout in their experiments. They correlated CHF with the liquid flow rate at the entrance to the test section and found that for very low flow rates (less than .01$\#_m$/sec for water) CHF was essentially a film dryout phenomenon, while at larger rates burnout was due to liquid hold-up caused by flooding in the annular gap. This at least qualitatively agrees with the findings of Schumann (6) and it should be expected that flooding will play a part in counterflow CHF, at least in some range of flow rates (or void fraction, etc.). Shires, Pickering and Blacker also developed a flooding correlation for a vertical annulus in which they found that tube length had an insignificant effect on flooding. Flooding in their work was defined as the vapor velocity which caused the liquid film to be stripped off the heated surface.

Recently Sakhuja (9) examined the role flooding plays in CHF in wickless heat pipes. The geometry of the wickless heat pipe is very similar to that of a closed end vertical tube open at the top to a large reservoir, the geometry examined by Schumann. Again, counterflow was caused by the rising vapor displacing downward the same weight flow of liquid. Using DoWtherm A as the working fluid, Sakhuja found that the maximum heat flux was constrained by flooding. Specifically he expressed his flooding cor-

relation (in the form of eq. 36) in terms of the heat flux assuming equilibrium flow (eq. 12) and the fact that the weight flow of liquid and vapor are equal. He concluded that the resulting equation represented the limiting factor of the range of data taken, and that CHF predicted by the flooding constraint agreed with experimental results. Sakhuja also compared the film boiling constraint (hydrodynamic instability) to flooding and found that for his data flooding was the limiting consideration (i.e., CHF due to flooding would occur before a hydrodynamically induced CHF).

Several methods exist in the literature for calculating counterflow void. Most of the correlations are expressed in terms of superficial velocities. Wallis (1) solved the momentum equations for a vertical falling film, assuming laminar flow, and related the film thickness to the void fraction. Zuber and Findlay (10) developed the Drift Flux Model for determining void, the results of which could be applied to any flow regime (slug, bubbly, annular) in any flow configuration (upflow, downflow, or countercurrent flow). The results were expressed in terms of the volumetric flux density (eq. 8) and the vapor drift velocity defined as,

$$u_{gj} = (u_g - u_f)(1-\alpha) = K_1 K_3 \sqrt{g D_o} \qquad 13$$

where Griffith has shown that $k_1 * k_3$ is approximately .35 (to be discussed later) as shown in reference 11. Zuber (2) determined expressions for u_{gj} appropriate for the slug, bubbly, and annular flow regimes. Griffith (11) determined that as long as gravity and inertia forces dominate u_{gj} assumes the form shown on the far right hand side of eq. 13. In any case, by observing

appropriate signs in the Drift Flux Model expression for void (eq. 30) the resulting expression could be used to predict counterflow void fraction. This has been done and the results will be discussed.

1.6 Scope of Research

The void fraction as defined by eq. 1 gives a direct measure of the amount of vapor , and hence liquid $(1 - \alpha)$, present in a system. Liquid serves as the cooling agent. Reducing the amount of liquid (i.e., the liquid fraction) will also reduce the critical heat flux. The assumption is then that CHF can be correlated with some parameter which gives a measure of the amount of coolant present. Either the flowing quality or the void fraction provides such a measure. But since in countercurrent flow the void is well defined while the flowing quality(vapor flow rate divided by total flow rate) is not, void fraction was thus the correlating variable used in counterflow CHF. This heuristic argument formed the basis for this investigation - to determine what the relation was between CHF and void.

Specifically the purpose of the program was to experimentally determine the following:

1) a correlation for CHF and void fraction in countercurrent flow;

2) the limits of the counterflow region in terms of liquid and vapor velocities;

3) the relation between counterflow CHF and pool boiling from a vertical surface;

4) the void range at which counterflow CHF could be approximated by pool boiling from a vertical surface;

5) how well void fraction could be computed from pressure drop data, and how measured voids compare to those calculated using the Drift Flux Model appropriate to countercurrent flow;

and 6) how counterflow CHF compares or is related to CHF in upflow or downflow.

To determine the above, the following parameters were varied:

1) the outer diameter of the vertical annulus, holding the diameter of the internally heated cylinder constant;

2) test section length (L in fig. A)

and 3) liquid velocity.

The range of operation and test section parameters were the following:

Heated lengths - 1.0 and 2.0 inches;

Liquid mass flux out of test section - 0 to $3.0 \times 10^5 \#_m/hr\text{-}ft^2$ (or 0 to .50ft/sec);

Outer shroud diameter - .474in. to 5.375 in.;

Heater diameter - .40in. (o.d.);

System pressure - approximately 1atm.;

Power - direct current heating ;

Heater material - Inconel 600.

It is to be noted that the liquid velocity specified above is the velocity leaving the annulus (j_{f1} in fig. A). This velocity is much easier to vary and measure than the inlet velocity (j_{f2} in fig. A) because at the inlet to the annulus, a two phase mixture is present while at the outlet only the single phase liquid is present. The inlet liquid velocity into the test section cannot

be measured á priori using conventional flow meters, but the flow rate out of the test section where only single phase liquid is present can be measured and kept constant while taking data. In cocurrent upflow experiments the characteristic liquid velocity is usually the liquid entering the test section where single phase liquid is always present. In vertical counterflow the characteristic velocity is the velocity at the liquid exit.

CHAPTER II

EXPERIMENTAL PROGRAM

2.1 Test Section Geometry

The principle geometry examined here was that of an internally heated vertical annulus. Of course both walls of the annulus could have been heated, but the internally heated annulus simulated adequately the geometry of an isolated fuel rod inside a reactor pressure vessel. More specifically, the corner rod in a rod type fuel bundle is best modeled by a vertically oriented annulus. The problem then was to isolate the boiling characteristics of a single rod and determine to what extent the void fraction could be used to predict CHF in this geometry.

Compared with all other possible fuel cell geometries, the annulus has the highest and in fact the limiting ratio of unheated to heated surface area (12). It should therefore giwe the lowest CHF value since burnout has been found to be reduced in the presence of an unheated surface. Lienhard and Keeling (13) pointed out that a flat ribbon heater in natural convection boiling induced strong side flows and that when these side flows were blocked by vertical walls, CHF was much lower than when the side flows were allowed. Also, Becker and Hernborg (14) reported that CHF values in an internally heated vertical annulus in upflow were lower than in round tubes or in a dual heated annulus (both internal cylinder and outer shroud heated). They attributed this difference to the fact that only a fraction of the channel perimeter was heated. Thus it is seen

that any CHF correlation resulting from data taken in the vertical, internally heated annulus, will be conservative when compared to other geometries. This is a desirable chatacteristic of this geometry.

In all experiments run, countercurrent flow was set up by the action of rising vapor produced from boiling on a heated surface flowing against a down current of liquid, the down current being either forced or induced (what Tong (15) describes as a natural circulation loop).

A program was also run to determine counterflow CHF in a round tube. The geometry tested was actually an extension on the work performed by Schumann (6) in that the vertical tube was opened at the bottom to permit a net down flow of liquid (when there is no net liquid flow out of the test section - natural convection counterflow boiling - the flow picture is the same as that reported in reference (6)).

The problem with the round tube geometry is that (as Schumann verified) with smaller tube diameters (around .50inch i.d.) flooding is the main cause of CHF. That is, low void steady-state CHF data is difficult, if not impossible, to obtain in small diameter tubes. In fact, in order to eliminate the effects of flooding in the round tube experiments (reported in Appendix B), it was neccessary to have the heated lengths so short that end effects predominated. In any case the flow pattern set up in a round tube is one of an annular type flow with a jittering rough liquid film flowing down the tube wall. This

oscillatory motion results in large pressure and hence void fluctuations and leads to a larger error in CHF detection. This is so because a dry patch formed is quickly cooled by liquid splashing on the heated surface. The result is that CHF as a film boiling phenomenon never occurs. The results of the round tube program nevertheless qualitatively agreed with the fact that in the low void region, CHF is usually a result of a hydrodynamic instability, while in the high void region (greater than around 80%) both flooding and film dryout are possible CHF mechanisms. Also, the results of the round tube program did show that CHF in an annulus was indeed lower that CHF in a round tube.

2.2 Choice of Working Fluid

If one desires to properly simulate the conditions in a reactor core at the onset of a LOCA, a full scale cluster of electrically heated rods contained in a vessel capable of sustaining pressures of around 1000psia would have to be built. The size, high pressure, and power requirements of such a rig would be costly and bulky to operate. For this reason it is desirable to consider the design of a small scale apparatus with lower power requirements. The criterion which determines the size of this apparatus is governed by the working fluid. Also the utility of the results obtained from the model apparatus depends on the accuracy of scaling laws which relate the model data to water data obtained under "similar" conditions but at higher pressure. Freon 113 was chosen as the working fluid because such laws are known, it is safe to work with, and its latent heat of

vaporizarion is relatively low at atmospheric pressure.

While it is not intended here to give a detailed explanation of Freon 113-water scaling, a brief discussion follows illustrating how the pertinent dimensionless numbers might be utilized to design a model apparatus.

Well known dimensionless groups for scaling were developed by Zuber (16) assuming equilibrium flow in circular tubes. The continuity, momentum, and energy equations were linearized and the following dimensionless groups resulted from the analysis:

$T = \rho_f / \rho_g$	density ratio	14,
$Z = L/D$		15,
$Vr = u_{gj}/u_i$	ratio of vapor drift velocity to inlet liquid velocity	16,
$Re = \frac{u_i D}{\nu_f}$	Reynolds number based on saturated single phase liquid flow	17,
$Fr = g L/u_i^2$	Froude number	18,
$Sc = \left(\frac{\rho_f}{\rho_g} - 1\right)\left(\frac{h_f - h_i}{h_{fg}}\right)$	subcooling number	19,
and $Pc = \frac{q'' 4 L}{h_{fg} u_i D (\rho_f - \rho_g)}$	phase change number	20.

T, the density ratio in eq. 14, is a measure of the system pressure. Pc represents the amount of vapor generated (assuming equilibrium flow). Sc is a measure of the degree of inlet subcooling. And Vr is a characteristic of the flow regime.

Crowley and Bergles (17) showed how the above groups could be used as appropriate scaling laws for modelling an apparatus with water as the working fluid by one using Freon 113 with the main objective being a reduction of the system pressure and

power requirements while still maintaining similar dynamic and thermal behavior. In this scaling procedure, the model and prototype are geometrically similar since this would help insure that the flow regime is similar. The procedure they used is detailed in reference 17. Briefly the scaling was achieved by requiring similarity of the dimensionless groups given in eqs. 14 to 20 in both model and prototype. The results of their modelling procedure applied to a prototype with water as the working fluid at 1000psia is given in Table I below:

Table I

	Water	Freon 113
P	1000psia	131psia
D	1.0in.	1.315in.
L	15ft.	19.7ft.
u_i	5.0ft/sec	5.75ft/sec
$(T_s-T_b)_i$	50F	20.5F
q"	294,000Btu/hr-ft^2	52,500Btu/hr-ft^2
X_o	30%	30%
ρ_f/ρ_g	20.7	20.7
L/D	180	180
Re	302,000	302,000
Fr	19.3	19.3
Sc	1.81	1.81
Pc	7.67	7.67

From Table I it is seen that the desired scaling has been achieved- a reduction in pressure and power requirement.

For counterflow in an annulus it has been found that pool boiling from a vertical surface represents an upper limit to CHF. An examination of the relative values of the maximum heat flux in pool boiling for water and Freon 113 can then be expected to give an indication of the power requirements of Freon compared to water and help decide whether Freon 113 would be an appropriate

fluid to use in the model apparatus. For pool boiling from a vertical surface in a centrally heated annulus, Zuber's well known flat plate prediction, q_{maxz} in eq. 21 below, is used and plotted against pressure in fig. 11.

$$q_{maxz} = .131\, h_{fg}\, \rho_g^{1/2} \left[\sigma g g_c (\rho_f - \rho_g)\right]^{1/4} \quad \text{---(24)} \quad 21.$$

Fig. 11 shows that for water pressures from around atmospheric to 1000psia, Freon 113 pool boiling values are from 8 to 10 times lower than the corresponding water values which compares to a reduction by about a factor of 6 predicted from the scaling laws of eqs. 14 - 20 and shown in Table I.

All Freon 113 properties were taken from the literature published by E.I. duPont & Co. In all Freon calculations the property values used are those given in Table II below.

Table II

$\rho_g = .457 \#_m/ft^3$
$\rho_f = 94.35 \#_m/ft^3$
$h_{fg} = 63.17 Btu/\#_m$
$\sigma = .00111 \#_f/ft$
} 1atm.
$T_{sat} = 117.6F$
$T_{crit} = 417.4F$
$P_{crit} = 498.9psia$
$\mu_g = .0108$ centipoise
$\mu_f = .510$ centipoise

2.3 Description of Apparatus and Flow Loop

Schematic diagrams of the flow loops are shown in figs. 5, 6, and 7 (fig. 7 will be discussed in Appendix B). Fig. 5 shows

the loop plumbing for the counterflow experiments, and fig. 6 illustrates the upflow plumbing. Only slight modifications to the counterflow loop were neccessary to reverse the direction of the inlet liquid.

All piping and fittings were ½inch "poly flow" tubes and fittings. Flow circulation was provided by an Eastern Industries type P-1 pump. A small wire mesh was fitted inside the pump inlet to collect particles of dirt, etc. The boiler consisted of a 10inch i.d. circular steel cylinder. Fitted to the bottom of the cylinder was a Hottwatt (Danvers, Mass.) no. Is754 immersion heater providing the heat required to bring the Freon in the boiler up to saturation temperature. A Pyrex glass condenser was installed on the cylinder top plate, open to the atmosphere, and was found sufficient to condense the Freon vapor generated by the immersion heater.

Rather than directly condense the vapor generated by the test section, a means of simply removing or bleeding the vapor from the liquid vapor outlet was provided (shown in figs. 5 and 6). This method neccessitated that Freon be supplied periodically to the loop to replace the quantity lost by evaporation (strictly speaking, the loop is not closed). The supply tank served this purpose. When the two phase mixture entered the supply tank, the vapor would rise and be condensed (or lost to the atmosphere) by a Pyrex condenser installed at the top. The outlet line of the supply tank was located at the bottom to insure that only single phase liquid would be pumped into the boiler

(the outlet line from the boiler to the pump was also located at the bottom to insure that liquid only would be pumped into the test tank). The supply tank was a 7 inch diameter by 15inch high neoprene circular container with 1/2inch "poly flow" fittings installed on opposite sides on the bottom.

A preheater was installed at the pump outlet to provide a fine adjustment of the Freon temperature entering the test tank. This preheater was made from a 1.0inch i.d. by 18 inch long copper pipe with heating tape (Cenco no.16596-2, 86watt capacity) wrapped around the surface of the cylinder. The inclusion of this preheater was neccessary to insure that Freon entering the test tank would be at or close to saturation. It was, however, neccessary to admit to a certain amount of subcooling in order to avoid boiling in the preheater.

Power to the test section was provided by an L.J. Land & Co. portable d.c. generator. The generator served as a direct current power supply, as the heater was a resistance type heater. The current to the test section could be regulated through a control console. The volt and current meters provided on the console were not sufficient to provide the desired sensitivity in current readings, however, since the maximum current drawn from the generator was never greater than 350 amps and the meter provided ranged from 0-3000amps. As a result a new 0-350 amp Weston ammeter was installed and was sufficient to provide the desired accuracy in current readings ($\pm$ 2% maximum scale).

The entire loop was mounted on a Dexion support frame, and

all tests were run in the MIT Heat Transfer Laboratory. A photograph of the entire flow loop is shown in fig. 8a.

2.3.1 Test Section and Test Tank

Figs. 8b and 9 show a close-up photograph and schematic diagram respectively of the test tank symbolized in figs.5 and 6 (insulation has been removed for clarity in fig.8b). Some difficulty was experienced in the test section design since it was desired to design an annular test section with a variable outer shroud diameter. The difficulty arose in requiring that the test section be enclosed within and electrically insulated from a container and still provide a means of changing the outer shroud. The final design consisted basically of two glass cylinders sandwiched between three aluminum and brass plate via eight connecting rods. The glass cylinders were 6.0 inch i.d. and 5/16 inch thick. The top and bottom cylinders were 6.0 inches and 2.5 inches long respectively.

To provide a means of changing the outer diameter of the test section, a number of aluminum disks, 5.0 inch o.d. with different i.d.'s, were machined with thicknesses equal to the heated lengths examined (1.0 and 2.0 inches). The disks were made to sit on an o-ring which in turn was fitted into a groove cut in an aluminum shelf (see fig. 8b) so that the only flow permitted was in the annular gap. Two "J" bolts were attached to each disk to provide a means of lifting the shroud out of the test tank.

Rather than completely disassemble the entire test tank

each time a new shroud was replaced, a removable top plate (fig. 9) was designed so that easy access to the inside of the test tank and the shroud disk could be provided by simply removing a few bolts rather than disconnecting all eight connecting rods and dismantling the entire test tank. The removable top plate was attached to the top plate by eight screws symmetrically tapped around the circumference of the top plate (this can be seen in the top of fig. 8b). The removable plate was a 1/4 inch thick by 6-5/8 inch diameter aluminum disk. The top and bottom plates were both 3/8 inch thick by 8 inches diameter brass disks with eight 1/4 inch holes drilled symmetrically around the circumference for the 8 connecting rods. The glass cylinders were fitted into grooves cut in the plates and sealed with Buna-n rings.

The aluminum shelf, situated between the two glass cylinders, was designed to provide a "seat" upon which the shroud disks could be placed, and to provide the location for the pressure taps (the taps could not be placed in the glass cylinders). This shelf was 2.0 inches thick and 7 inches in diameter with a 5-3/8 inch hole machined in the center to a depth of 1.5 inches (the shelf). A hole was machined to 4.25 inch diameter to permit liquid flow out of the annular gap. The glass cylinders were fitted into grooves cut in the top and bottom of the aluminum shelf and sealed with Buna-n rings.

Three 3/32inch diameter pressure tpas were drilled in the side of the aluminum shelf (shown in figs. 8b and 9). The bottom

and middle taps were used for pressure measurements in the 1.0 inch test section (shroud disk thicknesses were 1.0 inch), and the bottom and upper most taps were used in the 2.0 inch heated length experiments (2.0inch shroud disk). Depending on which heated length was used, either the top or middle tap was connected to the pressure gage via 1/4inch "poly flow" tube and fittings (the tap not in use was blocked up).

The bus bar of the resistance heater was electrically insulated from the top removable plate and the bottom plate by two nylon bushings attached to the plate and sealed with o-ring seals (clearly visible in fig. 8b). Screwed into these bushings were 1/2inch "poly flow" straight fittings drilled out to the o.d. of the copper bus bar and with o-rings used as the seal instead of the plastic ferrel provided. The entire test section assembly was made to fit inside these fittings. A close examination of fig.8b will reveal this design.

The test section assembly consisted of two copper rods, .50inch in diameter and 8 inches long, tapered at each end to .40 inches. The tapered ends were silver soldered to each end of an Inconel 600 cylinder (.40inch o.d., and .346inch i.d.). For each heated length (1.0inch and 2.0 inch heated lengths) such an assembly was required.

As shown in fig. 9, the heated section is filled with Al_2O_3 ceramics in which is placed the thermocouple beads. The thermocouple leads were threaded through a 1/8inch hole drilled in the top copper bus bar (shown in fig. 9). The only difficulty arising from this design was that each time a shroud disk was

changed, the thermocouple leads had to be disconnected from the multipoint switch to allow the removable top plate to be completely lifted out and away from the test tank to provide access to the inside.

The test section assembly was supported in the test tank by the 1/2 inch ploy flow fittings as shown in figs. 8b and 9.

It should be noticed in fig. 9 that the actual annular geometry is the heated section enclosed within the center hole of the shroud disk. The only flow permitted between the upper and lower plenum of the test tank is through the annular gap. Also, the only flow permitted to enter or leave the test tank is via the liquid-vapor outlet, liquid inlet, and liquid outlet shown in fig. 9.

2.3.2 Instrumentation

The pressure across the test section was measured by an inclined manometer (Ellison draft gage, 0 to 1.5inches). The manometer fluid was Meriam no. 3 fluid having a 2.95 sp.gr. ($184\#_m/ft^3$). The manometer was connected to the test tank via a 1/4 inch "poly flow" tubes and fittings. The pressure was measured by simply recording the height of the Freon-oil interface as measured by the attached scale on the gage body. The pressure could be read to within ±.01inches. The recorded value was subtracted from the zero initial value with no boiling, and the difference represented the pressure due to boiling. The Freon-oil interface was steady at low voids but somewhat oscillatory in the high void range (greater than 80%). The accuracy in pressure readings in this region was therefore not as great as at lower

voids (pressure oscillations in the high void region could result in as much as a 30% change in void fraction). This high void pressure oscillation was probably due to the onset of flooding.

The basic temperature measurements were made by copper-constantan thermocouples made from 24 gage Leeds and Northrup wire. The test section inlet temperature was measured by a thermocouple placed directly in the upper plenum of the test tank via a Conax packing gland. The heater temperatures were measured by three thermocouples placed on the inside of the thin walled Inconel cylinder (the heater), and the space between the thermocouple beads and the inner wall was filled by Al_2O_3 ceramics to prevent electrical noise in thermocouple measurements. All of the thermocouples were connected to a common junction through a multipoint switch. The output appeared on a Triplett model 4235-F digital volt meter. This meter greatly facilitated temperature readings in that wall temperature rises could be more easily and quickly detected on the digital panel than on a conventional potentiometer. The meter was initially calibrated to within .01 millivolts.

A Fischer-Porter flowmeter was installed at the test tank outlet (inlet for upflow loop of fig. 6) which measured the liquid volume flow rate out the test section. A variety of floats provided measurement of the test section flows up to $1.3 \times 10^{-3} ft^3/sec$. The meter was calibrated beforehand by measuring the volume of liquid collected in a specified time. After installation, the results were periodically checked against the initial callibration.

The heat input to the test section was calculated from measurements of the current, I, to the test section. Since,

$$q = I^2 R \times (3.413) \text{ - in Btu/hr} \qquad 22a$$

and

$$R = \rho_r L / A_{x\,heater} \qquad 22b,$$

knowing the resistivity, ρ_r, and current determines q. For Inconel 600, $\rho_r = 4.05 \times 10^{-5}$ ohm-inch and is approximately constant over the range of heater wall temperatures which were measured in the experiment (72F to 250F). The total heat input could also be computed from the voltage drop across the test section, i.e.,

$$q = V^2/R \times (3.413) \text{ - in Btu/hr} \qquad 22c.$$

But since the instrumentation required to obtain voltage measurement is potentially difficult to set up (at least in design), eqs. 22a and 22b were used to calculate the heat input from the measured current.

For the following heater dimensions, the corresponding resistances, R, are given below:

i.d. = .346inch o.d. = .40inch L = 1.0inch	.00126 ohm	i.d. = .346inch o.d. = .40inch L = 2.0inch	.00256 ohm

2.4 Experimental Procedure

The critical heat flux may be approached in two ways. In the first method the surface heat flux is kept constant and the liquid flow rate is gradually decreased until CHF occurs. In the second and more common method, the desired flow conditions are kept constant while the heat flux is increased till CHF occurs. In this study the second method was used.

First the liquid velocity out of the annulus (for the counterflow tests) or into the annulus (upflow) was set by an appropriate adjustment of v1 (figs. 5 and 6). Then power to the boiler immersion heater was turned on to bring the flowing Freon temperature as close to saturation as possible. The manometer lines were checked to make sure that all air in them was purged prior to each run. The Freon temperature was allowed to reach steady state, taking about one hour. Once steady state conditions had been reached, the preheater was adjusted to bring the temperature of the Freon entering the upper plenum of the test tank as close as possible to Freon saturation temperature. This usually required an additional 15 minutes. Once the final inlet temperature had been established, the current to the test section was slowly increased in increments of 20 amps. Between each power setting, the temperature was allowed to reach its steady state value, requiring usually 10 minutes between power increases. At each step in power level, the heater and inlet temperatures and pressure were recorded. The power was then increased in steps until CHF occured. Once the CHF point was reached, the power was decreased by 40 amps and then slowly increased in smaller steps to get a more accurate heat flux value.

When burnout did occur, the power to the test section was quickly turned off. A new liquid flowrate was chosen and the procedure repeated.

Data was taken in this way for each shroud diameter.

2.5 CHF Detection

The principle way in which CHF was detected was through the use of thermocouples. At CHF a wall temperature rise was indicated by the digital volt meter. This temperature rise was very rapid, reaching nearly 300F in a matter of seconds (the maximum heater surface temperature recorded in steady state was around 150F). Consequently the digital volt meter was closely monitored during power increases to the test section.

Since the thermocouples were not actually attached to the heater surface, there may initially be some question regarding the time response of the thermocouples to an increase in heater surface temperature. Cermack et. al (18), in their analysis of burnout in rod bundles during pressure blowdown, measured the wall temperature of their electrically heated rods in essentially the same way as in this study - by inserting thermocouples in the center of each heater tube and then filling the tube with Al_2O_3 ceramics. An estimate of the time response of their thermocouples was demonstrated during their transient tests, and they found that the time response was at most .50 seconds. Since the wall temperature rise at CHF was very rapid, there was consequently no ambiguity in the CHF point.

Interestingly two other ways were found to be a reliable indication of CHF. The first was simply a visual observation of the heater. Prior to CHF the heater was in a state of nucleate boiling. Once film boiling was initiated, a vapor film was stabilized on the heater surface which was clearly visible. The

other and less obvious (and more restrictive) way of detecting CHF was a result of a pressure increase in the direction of the bubble motion in the nucleate boiling regime. Upon initiation of boiling, the pressure suddenly increased. This increase was thereafter gradual for step changes in power settings. At the onset of film boiling (CHF), however, the pressure quickly dropped and returned to a value very near its initial value. This phenomenon is the result of a reduction of vapor generation at CHF (and hence void fraction). For the larger shroud diameters (greater than about .75inch) the pressure reduction was as noted. However, a rapid reduction in pressure at CHF was not observed for the smaller shrouds (smaller than .75inch). This is so because for the smaller shrouds, the void fraction in film boiling is nearly the same as the void in nucleate boiling with the result being that a pressure change will not quickly occur at the onset of film boiling.

2.6 Reproducibility of Data

For each CHF point three runs were made to determine data reproducibility. The average of the three fluxes obtained was taken to be the CHF value for the particular flow conditions existing. In all runs the maximum error in CHF was ±5%.

Pressure measurements showed greater error for some shroud diameters. For the larger shroud diameters (greater than .75 inch) the pressure measurements were satisfactorily reproducible, usually to within at least ±10%. Also there were no oscillations of the Freon-oil interface of the manometer for shrouds down to around .75 inch, and the interface movement in the manometer was

smooth and steady,with power increases to the test section. For the .546inch and .475inch shrouds, significant oscillatory motion of the interface was noticed very near CHF. This motion could result in as much as a 30% change in the manometer height for the same set of flow conditions. Consequently for these shrouds, and especially with high liquid velocities down (around .35ft/sec), the interface oscillation was the greatest. This was probably due to the onset of flooding which is characterized by large pressure and flow oscillations.

All temperature measurements were reproducible to within ± 5%.

The entire test tank was insulated with fiber glass wool. Since an effort was made to bring the entering Freon temperature to saturation, heat losses due to cooling of the liquid by the test section heater were considered negligible.

Axial conduction heat losses from the heater to the copper bus bars were estimated by a worse case analysis. The results showed that heat lost in this way was less than 7% of the total power input, and is much less for most of the data taken.

CHAPTER III

RESULTS

3.1 Void Fraction and Pressure Drop

While void fraction is known to be one of the most important parameters of two phase flow, it is also one of the most difficult to measure. Boiling void data are especially difficult to obtain and predict.

In the boiling literature there appear many techniques for measuring void. The techniques fall into two categories: 1) direct measurement; and 2) indirect measurement (19). The direct methods include deducing void fraction from measurement of other parameters such as capacitance, electrical resistivity, thermal conductivity, etc. of the two phase mixture. Direct void measurement techniques include photographic studies of the system, sampling probes, and separation of the phases by "trap" type mechanisms. All of the above have certain disadvantages, if not in accuracy then in cost. Also, due to the size and geometry of the test section used herein, most of the above methods are impractical (e.g., use of the vapor trap technique would require a considerable design effort to implement). The scheme finally decided upon is potentially the simplest. It is based on the fact that void fraction is related to all three components of the total pressure in two phase flow. A discussion follows.

The total pressure drop (relative to the hydrostatic pressure) in two phase flow is given by the sum of three components: 1) the pressure due to frictional effects; 2) the pressure due

to a momentum transfer across the test section; and 3) the gravity pressure drop. That is,

$$\Delta P_T = \Delta P_g + \Delta P_m + \Delta P_f \qquad 23.$$

In all two phase systems the gravity component of eq. 23 is (assuming that the void is constant along the test length),

$$\Delta P_g = [\alpha \rho_g + (1-\alpha)\rho_f] L \frac{g}{g_c} \qquad 24.$$

The determination of the momentum and friction pressure drop depends on a detailed knowledge of the two phase flow configuration of interest. Several techniques exist with which approximations can be made for the friction and momentum pressure drop terms used in performing a force balance on an elemental section of the flow geometry. Among these techniques the most easily adaptable and applicable technique to countercurrent flow is that of separated flow theory. This theory permits the two phases to have differing properties and velocities. Using separated flow theory, there are two ways to carry out tha analysis: 1) a detailed analysis in which separate continuity and momentum equations are written, together with rate equations which describe how the phases interact with each other and the walls of the tube (1) and are correspondingly solved; and 2) allowing only a variation of the velocity between the two phases while the appropriate equations are written for the <u>combined flow</u>. In the second method no regard is given to the specific flow regime or flow details. The second and easier method was used here.

Now consider a control volume enclosing the two phase fluid of an annulus (fig. A on next page).

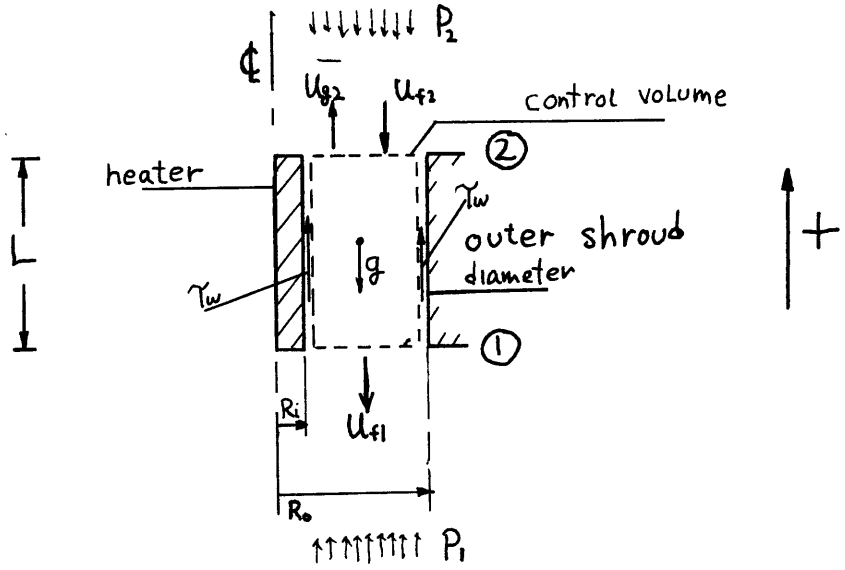

Figure A

The control volume assumes nothing specific about the division of the two phases, only that vapor and liquid leave the control volume at station 2 and 1 respectively and that liquid enters at station 2. Note that the wall shear stress indicated on the heated surface and outer shroud assumes the existance of a liquid film on both these surfaces (a liquid film on the heated surface was never actually seen).

In writing the continuity and force balance equations for the control volume of fig. A, the velocities of the liquid and vapor, u_f and u_g respectively, are assumed to correspond to separated flows through areas A_f and A_g. Then assuming that the pressure at any cross section is constant, a radially lumped force balance yields (observing the sign convention of page 9):

$$(P_1-P_2)A + \tau_w 2\pi R_o L + \tau_w 2\pi R_i L - \left(\rho_g \frac{g}{g_c} L A_g + \rho_f \frac{g}{g_c} A_f L\right) = \rho_f U_{g2}^2 \frac{A_g}{g_c} + \frac{U_{f2}^2 \rho_f A_f}{g_c} - \frac{U_{f1}^2 \rho_f A_f}{g_o} \qquad 25.$$

The effect of heat addition is accounted for by the momentum

term appearing on the right side of eq. 25.

The wall shear stress, τ_w, can be approximated by the wall shear assuming liquid only is flowing inside the annulus if the liquid velocity equals the average liquid velocity over the test length, and the friction factor is assumed to be .005 (1). Using this assumption and eqs. 4,5,6, and 7 substituted in eq. 25 gives the force balance in terms of the known superficial velocities (assuming equilibrium flow where eq. 12 applies), $P_1 - P_2$ (the total measured pressure drop), and the unknown void fraction:

$$\Delta P_T = [\alpha \rho_g + (1-\alpha)\rho_f]\frac{g}{g_c} L - \frac{.01 J_{fA}^2 L}{g_c(1-\alpha)^2(D_o - D_i)} \qquad 26$$

$$+ \frac{J_{g2}^2 \rho_g}{g_c \alpha} + \frac{J_{f2}^2 \rho_f}{g_c(1-\alpha)} - \frac{J_{f1}^2 \rho_f}{g_c(1-\alpha)}$$

where $J_{fA} = (J_{f1} + J_{f2})/2$. The three components of eq. 23 can be identified as follows:

$$\Delta P_f = \frac{-.01 J_{fA}^2 L}{g_c(1-\alpha)^2(D_o - D_i)} \qquad 27,$$

$$\Delta P_m = \frac{\rho_g J_{g2}^2}{g_c \alpha} + \frac{J_{f2}^2}{g_c(1-\alpha)} - \frac{J_{f1}^2 \rho_f}{g_c(1-\alpha)} \qquad 28,$$

and where eq. 24 gives ΔP_g.

The continuity equation in countercurrent flow written in terms of superficial velocities for the control volume of fig. A is,

$$J_{f2} = J_{f1} - J_{g2}\frac{\rho_g}{\rho_f} \qquad 29.$$

Equation 26 is not meant to be a highly accurate and ana-

lytical expression for counterflow void. The success of using eq. 26 depends in large part on the magnitude of ΔP_g, ΔP_f, and ΔP_m. In regions where eqs. 27 and 28 are significant compared to eq. 24, the void will not be accurately predicted by eq. 26. This is so because eqs. 27 and 28 depend on the assumptions made of the detailed flow regime and the way in which j_{g2} is measured for boiling systems. In the actual pressure measurements it was observed that in the high void region, greater than about 75%, the manometer interface would exhibit smooth but significant oscillations (as already noted) making readings more difficult. It is expected that in this region the void fractions calculated from eq. 26 are not very accurate, and ΔP_g, ΔP_f, and ΔP_m, are of equal magnitude. Fig. 10 shows that the friction and momentum terms can be significant compared to ΔP_g at high voids (75% to 80%). For voids less than about 75% the friction and momentum terms are negligible compared to the gravity pressure drop of eq. 24. Eq. 23 with $\Delta P_T \approx \Delta P_g$ then provides the proper expression for estimating the void fraction.

It is important to point out that the data presented here for pressure drop were taken with a single set of pressure taps immediately bounding the test section. As such the measured values represent an <u>overall integration</u> of the local pressure gradient over the entire heated length. This means that the void fraction calculated from eq. 26 is an average value since the data obtained really do not allow an estimate of the detailed pressure gradient.

An estimate of the local void can be obtained from the generalized expression for void fraction predicted by the Drift Flux Model, modified by Griffith (11),

$$\alpha = \frac{J_g}{\bar{J}(1+K_2) + K_1 K_3 \sqrt{g D_o}} \qquad 30.$$

The physical significance of the constants, K_1, K_2, and K_3 were explained by Griffith (11). Briefly, K_1 is a function of Reynolds number if surface forces are considered to be important (otherwise it depends on geometry), K_2 represents the ratio of mean to centerline velocity in a tube, and K_3 depends on the heat flux ($K_3 = 1.6$ for heated pipes and 1.0 for adiabatic systems). The constants K_1 and K_2 were expressed in terms of D_i/D_o for annuli and the values tabulated in Table III in Appendix A.. Using this table and eqs. 9 or 11 for up or counter flow, eq. 30 can be used to provide an estimate of either the local or average void fraction if the superficial velocities are known at any location along the heated length. Since film boiling was initially observed to begin at the test section exit (station 2 of fig. A), the void at the exit can be predicted from eq. 30 if the superficial velocities are known there.

In using eq. 26 to calculate the void, the assumption of equilibrium flow, eq. 12, was used to calculate j_{g2}. At low voids this is not a very good assumption. Fig. 3 shows this (the void fraction in fig. 3 was obtained from eq. 26 and the total measured pressure drop and hence is the average void along the entire heated length) in which it is seen that there is a

significant deviation between the modified Zuber-Findlay line (10) and the measured voids assuming equilibrium flow. All points falling above the dotted line and which are considered to be poorly predicted by the Drift Flux Model are voids less than about 50%.

An estimate of the local void fraction using eq. 30 was calculated by assuming a linearly varying profile for j_g, integrating eq. 30 over the heated length, and setting the resulting value equal to the average void predicted from eq. 26. The value of j_{g2} found in this way was then substituted back in eq. 30 to obtain thw local void. That is,

$$J_g = J_{g2}\frac{x}{L} \qquad 31.$$

Then, substituting eq. 31 into eq. 30 and integrating,

$$\alpha_{average} = \frac{1}{L}\int_0^L \frac{J_{g2}\,x/L}{\left(J_{g2}\frac{x}{L} - J_{f2}\right)(1+K_2) + K_1K_3\sqrt{g\,D_0}} \qquad 32$$

with the result that

$$\alpha_{average} = \frac{1}{1+K_2} + \frac{J_{f2}L(1+K_2)+LK_1K_3\sqrt{gD_0}}{J_{g2}(1+K_2)^2L}\ln\frac{J_{f2}L(1+K_2)+LK_1K_3\sqrt{gD_0}}{J_{g2}(1+K_2)L + J_{f2}L(1+K_2)+K_1K_3\sqrt{gD_0}} \qquad 33$$

The only unknown in eq. 33 is j_{g2}. The values of j_{g2} calculated from eq. 33 were, for some voids, somewhat absurd ranging from .10 ft/sec to over 100ft/sec. But as seen in Table IV the local void is always higher than the average void fraction (calculated from eq. 26) for all the data. The local void, it is to be remembered, is the void at the test section exit where j_{f2} and j_{g2} are known. Griffith (11) showed that at high vapor velocities,

a limiting void is obtained from eq. 30 of about 83%. Eq. 33 should not then be expected to provide an accurate measure of void beyond this value. Also, as mentioned, eq. 26 does not predict voids accurately greater than about 80%. Within these limits, the local and average void can be calculated from eqs. 33 and 26 respectively. Eq. 30 can also be used to calculate the average void fraction assuming equilibrium flow. This has been done and the results shown in fig. 12. It is seen that within the range of applicability of each method, calculated average voids are consistently higher than measured average voids up around 50% void. Greater than this value the data assume a normal distribution around the ideal which is consistent with fig. 3 where for voids less than 50%, a deviation from the Drift Flux model (eq. 30) is significant.

It is important to point out that the data appearing in fig. 3 do not account for the possible effects of vapor flashing along the heated length. This effect can be important even in very short heated lengths where a small pressure drop can cause significant vapor formation (increasing local void). Therefore the apparent deviation of the data in fig. 3 from the form predicted by the Drift Flux Model (eq. 30) is most likely due to two considerations; 1) the assumption of equilibrium flow; and 2) the effect of vapor flashing which theoretically causes increasing local voids at the test section exit (station 2 in fig. A) Zuber et. al.(2) have shown that the data appearing in fig. 3 are characteristic of the deviation to be expected

from the Drift Flux Model when no account is taken of vapor flashing along the heated length.

For the line drawn in fig. 3, $C_o = 1 + K_2 = 1.0$ and $u_{gj} = K_1 K_3 \sqrt{g D_o} = .90 \text{ft/sec}$.

3.2 Flooding

Countercurrent flow is complicated by flooding because it represents the transition from stable flow, to unstable flow, and back again. This was clearly observed in the round tube experiments when the flow changed from counterflow to upflow (flow reversal). During the transition, large pressure and flow oscillations were observed. After the transition was completed, the flow stabilized with a steady upflow of liquid film. Such flow instabilities were also observed in the transition from one flow regime to another (typically from the slug to annular flow regime). Again in the round tube experiments the transition was evidenced by large pressure instabilities. The liquid film exhibited a very turbulent, jiggling motion (much the same as was observed by Schumann (6)) periodically flooding the flow area and then being flushed through. Schumann identified this action as a "perculating" motion. Tong (15) has identified such flow instabilities in natural circulation loops as being the result of the elevation pressure drop being the dominant fraction of the channel pressure drop. In any case, once the gas velocity had reached a certain value (the flooding velocity), the vapor completely occupied the central core of the tube and the liquid film flowed down the tube walls - coun-

tercurrent annular flow.

Flooding has been typically described in the literature by use of nondimensional flooding velocities proposed by Wallis(20). He related the liquid and vapor velocities to the void fraction by a balance of buoyancy and frictional effects in the fluid. He then assumed that turbulent stresses were related to average momentum fluxes of liquid and vapor (i.e., the terms on the right hand side of eq. 28). The dimensionless groups which related these momentum fluxes to the hydrostatic forces were found to be the following:

$$J_g^* = J_g \left[\frac{\rho_g}{(\rho_f - \rho_g)\, g\, D_h} \right]^{1/2} \qquad 34,$$

and

$$J_f^* = J_f \left[\frac{\rho_f}{g\, D_h (\rho_f - \rho_g)} \right]^{1/2} \qquad 35.$$

These nondimensional velocities have special significance in countercurrent flow as mentioned since they relate buoyancy forces to the momentum transfer. They have also found use in up and downflow analysis, although in these flow configurations they lose their fundamental significance.

Most flooding phenomenon correlated with eqs. 34 and 35 have the general form shown below(1):

$$J_g^{*1/2} + m J_f^{*1/2} = C \qquad 36.$$

The constants m and C depend on fluid properties and geometry. Theoretically the constant m is proportional to the density

ratio, and C depends on the conditions under which the fluid enters the test line (e.g., for sharp flanged entrances, $C=.75$ and for rounded flanges $C=.88$). Hewitt and Hall-Taylor (4) have pointed out that m and C fall in the following ranges for a round tube:

$$.90 < m < 4$$

$$.70 < C < .90$$

In the round tube experiments with Freon 113 as the working fluid, the constants m and C were determined to be .934 and .682 respectively so that,

$$J_g^{*1/2} + .934\, J_f^{*1/2} = .682 \qquad 37.$$

Shires, Pickering, and Blacker (8) correlated flooding velocities with eqs. 34 and 35 using the hydraulic diameter based on both the rod preimeter, and rod and tube perimeter since in their experiments only the inner rod of an annulus was wetted before flooding. Except for the fact that they were concerned with film flow, counterflow in their experiments was basically the same as reported here - the fluid entering the test section flowed counter current to vapor boiled off the heated surface. Depending on whether the rod perimeter alone is used in the hydraulic diameter in eqs. 34 and 35 (D_h) or both rod and tube perimeter are used (giving the conventional hydraulic diameter for an annulus as $D_o - D_i$), the following correlations were arrived at:

$$J_g^{*1/2} + J_f^{*1/2} = .95 \qquad \text{rod perimeter only} \qquad 38.$$

or

$$J_g^{*1/2} + J_f^{*1/2} = 1.20 \qquad \text{rod and tube perimeter} \qquad 40.$$

Since in this study both the heated tube and outer shroud diameter were wetted before the onset of flooding, $D_o - D_i$ was used as the hydraulic diameter and consequently eq. 40 was used to describe flooding in an annulus.

Fig. 13 shows eq. 40 in relation to the counterflow data taken. It is seen that nearly all the data fall below the flooding line. The data which are closest to the flooding line exhibited the characteristics of flooding mentioned above. Also it will be seen that two points lie outside the counterflow region. These points were taken with the smallest shroud diameter examined (.475inch). Visual observations indicated that for these two points most of the vapor generated by boiling off the center cylinder of the annulus flowed out the bottom of the test section - station 1 in fig. A. This seemed to indicate that these data were very nearly in the downflow region.

The region outside the flooding line is not neccessairly the downflow or upflow region. It merely corresponds to the limit of the counterflow region, and outside this region either up or downflow can occur.

Since all data appearing in fig. 13 represent CHF points, it is realized that for some of the data, flooding was the mechanism causing CHF. For the round tube data (not shown in fig. 13) nearly all the data corresponded to flooding. - CHF was a result of flooding at the mouth of the tube. For the other data shown in fig. 13, the principle mechanism of CHF appeared to be the stabilization of a vapor film on the heated surface. The data closest to the flooding line in fig. 13 corresponded

to local voids of at least 75% indicating that flooding is basically a high void phenomenon.

3.3 Geometric Effects on CHF

The effects of geometry on CHF in upflow and some downflow are well documented in the literature. In countercurrent flow the data is scarce. Griffith, Schumann, and Neustal (7) reported a length and heater diameter effect on CHF in closed end vertical tubes. They found that for a given diameter, burnout increased with heated length up to a certain value and then remained approximately constant. Also, a diameter effect was noted in that decreasing the heated diameter for a given heated length and material causes burnout to occur at higher fluxes.

Lienhard and Dhir (21) explained the diameter effect on CHF in terms of hydrodynamic theory. They concluded that as long as the characteristic length of the heater was greater than about 6, pool boiling CHF would be unaffected by any further increases in this dimension. The characteristic length was defined as,

$$H' = H\sqrt{g g_c (\rho_f - \rho_g)/\sigma} \qquad 41$$

which is the square root of the Laplace number. Eq. 41 represents the ratio of buoyancy to capillary forces. The variable H is the characteristic heater dimension and is equal to the heater diameter for a cylinder, height for a vertical plate heater, etc. However, H really depends on the heater dimensions. That is, whatever dimension of the heater gives the smallest value of H' is taken to be the characteristic dimension (e.g, heater dia-

meter or length for a cylinder, or length or height for a vertical flat plate). Lienhard's results were verified from pool boiling data obtained from vertically oriented flat plate heaters with one side insulated (essentially the geometry shown in fig. 1c with the unheated surface removed). He presented his results as a plot of eq. 41 vs. a nondimensional heat flux defined as pool boiling CHF divided by q_{maxz} from eq. 21. This plot is shown in fig. 14. One data point from the annulus geometry is also included on this graph and represented the measured pool boiling flux from a vertical surface. Also shown in fig. 14 is one data point from the round tube program. This point corresponded to the smallest heated length examined (.10inch). The larger deviation of this point from Lienhard's prediction is probably due to the fact that CHF in the round tube experiments was essentially a high void phenomenon (fig. 4) while fig. 14 contains very low void data (less than 10%). Since pool boiling is essentially a low void phenomenon, it is somewhat inappropriate to try to explain the high heat fluxes obtained in the round tube program with a theory based on hydrodynamic instability. The very short heated lengths of the round tube program resulted in CHF values which were most certainly governed by end effects.

Also shown in fig. 14 is a data point taken from Costello and Adams (22) for a vertical cylinder, 3 inches long and 5/16 inch in diameter. It is seen that the point falls near the line predicted by Lienhard (21).

The conclusion to be drawn from fig. 14 is that at large characteristic lengths (length or diameter), q_{chf}/q_{maxz} is approximately 1.0. That is, eq. 21 can be used to provide an estimate of pool boiling CHF from a vertical cylinder (at saturation conditions).

For the annuli examined here, the principle geometric effect was that of varying the outer shroud diameter. Fig. 15 shows the variation of outer shroud diameter with CHF. It is seen that for the largest shrouds (D_i constant), the maximum heat flux is very nearly pool boiling from a vertical surface. The line drawn through the data points shown were taken in natural convection boiling which is the flow condition in pool boiling. The region below the curve of fig. 15 represents the region of forced convection boiling in countercurrent flow and the data shown below the line were taken with net liquid velocities down (u_{fl} in fig. A).

Since vertically oriented cylinders in an infinite pool of liquid can be considered an annulus (infinite outer shroud), the question which naturally arises is at what ratio of inner to outer diameter (D_i/D_o), or simply at what hydraulic diameter (D_o-D_i), does the pool boiling assumption break down? Shown in fig. 15 is that for $D_i/D_o \leq .3$ to .4 ($D_o-D_i \geq 1.3$inch) the pool boiling assumption is probably valid as these shrouds correspond to voids less than approximately 30% (see also Table IV). At values greater than about .4, however, the presence of an unheated surface moving closer and closer to the heated surface has the

effect of simply restricting bubble motion with the result that the bubbles tend to agglomerate more readily and form a vapor blanket at lower heat fluxes.

Shown in fig. 16 is the variation of CHF with liquid velocity from which it is seen that for increased liquid velocities down (for constant outer shroud diameter), CHF decreases in countercurrent flow and increases in upflow. One explanation for this is provided from fig. 17 where figs. 15 and 16 have been cross plotted. The data shown are for two selected diameter ratios cross plotted and are meant to provide an indication of the effect of liquid velocity on void. In countercurrent flow cooling of the heated surface occurs primarily by the bubble motion throwing liquid on the heated surface, while in upflow the through flow liquid motion is primarily responsible for cooling. This means that for increased liquid velocities down in saturated counterflow, the resulting restriction on bubble motion (upward bubble motion is impeeded by the downward movement of liquid) will increase the void fraction (fig. 17) and result in less liquid being thrown on the heated surface. CHF will then decrease with increasing liquid velocities as shown in fig. 16.

This effect of reduced bubble motion with increasing liquid velocities is more predominant at smaller shroud diameters where the flow area is greatly restricted. In fact, if the shroud is small enough, some bubbles can even be seen to reverse their direction creating a condition of partial downflow (some vapor would still be seen to flow up).

It is important to realize that these results have been verified only for flow near the saturation temperature of the working fluid. For significant degrees of subcooling, the above trends would not neccessairly be expected to apply since then thermal interactions between the two phases would probably be significant.

3.4 Critical Heat Flux and Void Fraction

From the preceding discussion parametric effects on CHF have been pointed out and illustrated in figs. 14 to 17. It is now apparent that CHF in countercurrent flow can be strongly influenced by liquid flow rates and varying outer shroud diameters. But CHF is not suitably correlated by these variables because it is not a single valued function of either. It must then be left to a perhaps more fundamental quantity to provide the proper correlating variable. The void fraction provides such a variable (or alternatively the "in place" quality, x_s, defined as the weight ratio of vapor to vapor plus liquid in the system (eq. 42 below)

$$X_s = \frac{\alpha \rho_g}{\alpha \rho_g + (1-\alpha)\rho_f} \qquad 42).$$

The fundamental result of this study is shown in fig. 19 where the void fraction has been plotted against CHF (q_{chf}/q_{maxz}). It is seen thereon that within the range of experimental error, CHF is a unique function fo void. The figure plots the local void as obtained from eq. 30 and 33. For each point plotted a line is drawn which indicates the relative magnitude of the local and average (eq. 26) void. The plotted point is the local

void while the left hand extension represents the average void calculated from the total measured pressure drop. The curve drawn through the data (local void) was obtained by the method of centroids.

From fig. 19 it is seen that CHF is relatively independent of void in the range 0 to 40%. In this range vertical surface pool boiling provides a reasonable estimate of counterflow CHF (i.e., approximately in the bubbly flow region). Beyond 40% void, CHF continually decreases with increasing void. This is entirely reasonable on physical grounds since the amount of liquid is decreasing with increasing void which would increase the CHF.

Beyond a void fraction of approximately 80%, the accuracy of void measurements at CHF greatly decreases due to increased pressure oscillations. This is not evident from fig. 19, and the region beyond 80% void has thus been indicated to remind the reader that beyond this void, the void fraction may not be accurate.

The pool boiling value which is approached with decreasing void fraction was experimentally obtained. Costello and Adams (22) measured pool boiling values from a variety of vertical cylinders immersed in a pool of distilled water. They found that pool boiling off vertical cylinders was nearly the same as the value predicted by eq. 21 for a horizontal flat plate (i.e., $q_{CHF}/q_{max} = 1.0$). The graph from which this was concluded was, however, of such a scale that it was difficult to deduce the ratio as being exactly 1.0, or .90, or 1.1, etc.

Based on the data obtained here, it was found that pool boiling from a vertical cylinder was approximately 84% of q_{maxz} of eq. 21, and that this value provided a low void upper limit to CHF in countercurrent flow in an annulus.

There are a number of points to note regarding fig. 19. The first is that the form of the void-CHF relation may be different for different geometries, orientations, pressures, and fluids. And while it is true that the data of fig. 19 include heated lengths of 1.0 and 2.0 inches as well as a variety of outer annuli diameters and flow directions, more work would have to be done to determine if the form of the relation would be altered if the heated lengths were, say, 5ft. or 10ft.

It has already been shown that geometry does effect the form of fig. 19 as evidenced by fig. 4 where for the round tube data, heated lengths as low as .10 inch were studied. But as the heated length is increased to 1.5 inches (and hopefully beyond) the data fall more nearly in line with the annuli data. Thus while there is every evidence to believe that the curve (or form) of fig. 19 corresponds to heater sizes considered to be outside the range of significant geometric effects on CHF (for instance as determined by fig. 14), more work would have to be done to ascertain this altogether.

Finally the idea that counterflow, or even upflow or downflow (since some upflow data is also included in fig. 19) Λ_{CHF} can uniquely be determined by the void, regardless of geometry, flow rates, or flow directions would greatly simplify heat flux

predictions in nuclear reactors since only a reliable method of determining the void fraction would have to be known.

CHAPTER IV

CONCLUSIONS AND RECOMMENDATIONS

4.1 Conclusions

An experimental investigation has been carried out to determine the critical heat flux in countercurrent flow in a vertical internally heated annulus using Freon 113 as the working fluid. The primary variable used in correlating counterflow CHF was the void fraction. A separate investigation was also performed to obtain CHF data inside a vertical round tube. For the low liquid flows and test section sizes examined, the following conclusions were drawn:

1) Counterflow CHF in a vertical internally heated annulus can be uniquely determined by the void fraction (or alternatively by the "inplace" quality as shown in fig. 18), and CHF increases with decreasing void. This conclusion is believed to apply to geometries beyond the range at which heater size significantly effects CHF (e.g., as determined from fig. 14);

2) For void fractions up to around 40%, pool boiling from a vertical surface provides a reasonable estimate of counterflow CHF. Beyond 40% void, CHF begins to drop off continuously with increasing void;

3) The observed location of CHF - the location at which film boiling was first observed to begin - was always at the top of the heated length (station 2 in fig. A). At CHF a vapor blanket was seen to quickly spread over the heated length making any detailed study of the location of burnout difficult;

4) The void fraction can be predicted from the total measured pressure drop as long as the gravity component dominates and the momentum and friction contributions are negligible. The resulting void will be an average void fraction over the region which the pressure is measured. In regions where the momentum and friction components are equal to the gravity term, the void will not be accurately predicted from pressure drop data. This region corresponded to voids greater than around 80% where eqs. 27 and 28 are nearly equal to eq. 24;

5) For liquid close to saturation temperature, counterflow CHF decreases with increasing liquid velocity down. The effect is just the opposite for upflow - CHF increases with increasing liquid velocity up;

6) For voids greater than 50%, the Drift Flux Model expression for void fraction can be used to predict counterflow void in boiling systems. For voids less than 50% there is a significant difference between void fraction calculated from the total pressure drop and the Drift Flux Model;

7) The limits of the counterflow region in terms of liquid and vapor velocities can be determined by the generalized flooding correlation of eq. 36. Both the round tube and annuli flooding data had the form of eq. 36 with eq. 40 providing the correlation for the annuli;

8) The region below the flooding line is the counterflow region while outside this line, either upflow or downflow is possible (fig. 12 shows two points outside the flooding line which were in partial downflow).

9) Counterflow CHF in an annulus is lower than in a vertical round tube, but for increasing heated lengths CHF for the two geometries showed evidence of falling on the same void-CHF curve (fig. 4).

10) It is not possible to obtain steady state CHF at low local voids inside small diameter tubes (less than 1.0inch) at saturation conditions unless the heated lengths are so short that the resulting vapor generated in boiling off the heated surface will not cause flooding at the mouth of the tube.

11) Flooding was found to be a high void phenomenon, occuring only at voids greater than from 75% to 80%.

12) For voids less than around 80% CHF is due to the onset of film boiling, while at voids greater than this value, flooding and film dryout are the main cause of counterflow burnout.

4.2 Recommendations for Further Study

The form of the void-CHF relation in counterflow needs more experimental verification if the results are to be applied to heater sizes, flow rates, and fluids other than those tested here. Specifically the following are recommended for further study:

1) A program to obtain void-CHF data in an annulus using a variety of fluids and degrees of inlet subcooling;

2) A program to determine the local void and CHF using a more sophisticated means of obtaining void data;

3) A model to analytically predict counterflow CHF in terms of void fraction;

4) A similar study as reported here to determine the form of the void-CHF relation at high pressures (around 200psia);

5) Designing an experiment to obtain low void counterflow CHF inside a vertical round tube for steady state heat input at saturation temperatures.

6) A program to determine in greater detail the relation between CHF in up, down, and counterflows.

Appendix A

Table III
(Constants appearing in Eq. 30)

D_i/D_o	(D_o in inches)	k_1	k_2
.0744	(5.375)	.348	.197
.315	(1.27)	.355	.187
.337	(1.186)	.358	.186
.400	(1.0)	.378	.182
.409	(.977)	.379	.182
.530	(.751)	.384	.174
.732	(.546)	.390	.156
.843	(.475)	.398	.144

Table IV
(Counterflow CHF in an Annulus)

D_o (in.)	L (in.)	q_{chf}/q_{maxz} $q_{maxz} = 64{,}925\ B/hr\text{-}ft^2$	$\alpha_{average}$ (eq.26)	α_{local} (eqs.30 and 33)	j_{fl} (ft/sec)	$\Delta P_t/L$ (lb_f/ft^3) (relative to elevation pressure drop)
5.375	1.0	.815	.0151	-	.00185	~94.35
5.375	1.0	.815	-	-	.00351	~94.35
5.375	2.0	.841	.0218	.041	.0157	90.35
1.27	2.0	.821	.257	.420	0.0	70.5
1.27	2.0	.752	.291	.464	.063	67.3
1.27	2.0	.714	.334	.513	.102	63.22
1.186	1.0	.815	.0527	-	0.00	~92.0
1.186	1.0	.717	.068	.132	.104	88.6
1.186	1.0	.795	.075	.143	.149	88.0
1.0	2.0	.667	.389	.572	0.0	58.31
1.0	2.0	.667	.423	.606	.0305	55.1
1.0	2.0	.623	.432	.614	.0558	54.2
1.0	2.0	.563	.517	.686	.109	46.1
.977	1.0	.815	.175	.307	0.0	78.7
.977	1.0	.767	.160	.283	.0322	80.1
.977	1.0	.757	.189	.328	.0589	77.25
.751	1.0	.422	.616	.756	.322	36.2
.751	1.0	.392	.572	.727	.367	40.4
.751	1.0	.341	.640	.770	.417	33.4
.751	1.0	.683	.352	.534	0.0	62.4
.751	1.0	.367	.680	.791	.231	30.5
.751	1.0	.496	.623	.760	.113	36.2
.751	1.0	.527	.518	.689	.0634	46.1
.751	1.0	.473	.503	.677	.116	47.5
.751	1.0	.610	.431	.614	.0226	54.6
.751	2.0	.558	.650	.775	0.0	34.6
.751	2.0	.374	.811	.843	.114	18.2
.751	2.0	.402	.762	.827	.0626	23.2
.751	2.0	.328	.794	.838	.223	19.1
.751	2.0	.303	.750	.822	.362	22.3
.546	1.0	.422	.790	.845	0.00	22.0
.546	1.0	.297	.829	.857	.183	14.9
.546	1.0	.274	.827	.856	.183	14.8
.546	1.0	.394	.696	.807	0.0	30.5
.546	1.0	.327	.804	.850	.115	19.22
.546	1.0	.335	.751	.832	.0471	24.9
.475	1.0	.255	.867	*	0.0	14.9
.475	1.0	.227	.806	.857	.377	3.44
.475	1.0	.225	.880	*	.135	7.74

Key: - negligible or not calculated
* no convergence of eq. 33

Table IV (contd.)

(Upflow CHF in an Annulus)

D_o (in.)	L (in.)	q_{chf}/q_{maxz}	$\alpha_{average}$	α_{local}	j_{fl} (ft/sec)	P_t/L ($\#_f/ft^3$)
1.27	2.0	.831	.164	.288	.0631	79.5
1.27	2.0	.873	.123	.226	.102	83.7
1.27	2.0	.840	.198	.342	.0316	76.3
.751	2.0	.614	.502	.676	.0625	48.5
.751	2.0	.616	.410	.595	.114	57.5
.546	2.0	.537	.568	.730	.329	49.36
.546	2.0	.475	.717	.817	.184	32.2

Appendix B

Description of Experimental Program to Determine CHF Inside a Vertical Round Tube

B.1 EXPLANATION OF APPARATUS DESIGN

A schematic diagram of the flow loop for this program is shown in fig. 7. All piping and fittings were 1/2 inch "Poly-flo" (lines 1, 2, 5, 6, 7, and 8 in fig. 7) except for lines 3 and 4 which were glass (.394 inch inside diameter) to facilitate visual observation of flow conditions at CHF. The air bleed line shown in fig. 7 served the purpose of removing the Freon vapor generated by the test section and preheated (PH2 in fig. 7). To replace the Freon lost by vapor generation, a small tank, open to the atmosphere and situated above the entire apparatus was included in the loop (fig. 7). This tank served as a kind of pressure equalizer to ensure that the loop pressure would stay at or near atmospheric. If the pressure in the loop becomes great enough, Freon will flow out the loop and into the tank (and vice versa).

It was necessary to include a preheater (PH1) in line 6 to insure that Freon entering the test section would be at or close to saturation (since care was taken to insure that the Freon entering the plenum was pure liquid, it was necessary to admit to a certain degree of subcooling in order to prevent boiling in PH1). This preheater consisted of a one inch inside diameter by 1.5 ft. long copper tube wrapped with heating tape capable of delivering 90 watts. This was found to be sufficient to keep the Freon entering the plenum from line 1 to within 5 degrees of saturation temperature (117).

The test section and PH2 were of similar design. They consisted basically of a circular copper disk, 1/2 inch thick by 3.5 inch diameter with a .394 inch hole drilled in the center and with three "Hotwatt" cartridge heaters placed in a symmetrical position (120 degrees apart) within the block. The blocks were sandwiched between two brass adapters, to which the glass tubing of lines 3 and 4 was connected via O-ring seals. The brass adapters were sealed and thermally insulated from the copper disks by teflon seals. The most important feature of the test section to point out is the length of the heated section, which for the .10 inch test section consisted of the block of

basic dimensions given above but with two 1.0 inch diameter by .167 inch deep holes cut into the top and bottom of the disk concentric with the .394 inch center hole, leaving only .10 inch of copper available as the heat transfer area, hereafter referred to as the .10 inch test section. The requirement for using such a small test length arises from the fact that as heat is added to the Freon in counter-current flow, vapor is generated in the test section in addition to the incoming vapor. This means that while the appropriate velocities of the incoming Freon liquid and vapor are chosen to be within the flooding limit of fig. 13, the additional vapor generated by the test section in approaching CHF causes, in some cases, the values of the incoming superficial vapor velocity to be increased by an amount sufficient to cause flooding at the test section outlet. Since equilibrium flow is assumed (equ. 12), reducing the heated length (a reduction to as low as .10 inch will increase the range of liquid flow rates which could be examined without flooding) is necessary to give some relatively low void data - data not obscured by flooding phenomena. Of course the validity of the results must be questioned since with such a small heated lenght, end effects predominate, and any conclusions drawn regarding CHF mechanisms or void-VHF correlations must be questioned.

The plenum (fig. 7) consisted of a 1.5 inch long by 3.5 inch diameter glass cylinder sandwiched between two brass plates by using five connecting bolts and sealed with 0-rings. To the bottom of the plenum was connected line three (fig. 7) and again the connection made via 0-ring seals.

In vertical tubes open at the top to a closed free volume, the possibility of geysering, or what Tong (15) describes as natural loop oscillations, occuring in the line exists if appropriate liquid or vapor flow rates are reached. It was shown by Griffith (23) that the condition for geysering to occur in a vertical tube is that

$$dP < 0$$

where dP is the pressure change of the column of liquid due to bubble formation. A relation between the pressure and the free volume above the column was developed by Griffith (23) and shown to be the criterion by which to predict whether geysering would occur. The conclusion was that if there is no free volume

(i.e. plenum filled completely with liquid) then geysering would not be likely to occur. This was observed to be true in this investigation, and the loop was designed to keep the plenum filled with liquid during each experimental run. When power was added to the test section and PH2, the subsequent vapor formed would rise in the column (lines 3 and 4) and enter the plenum, escaping via line 2 and into the air bleed and consenser. The liquid entering the plenum from line 1 was sufficient to keep the plenum completely filled with liquid (actually near CHF there was some vapor collection in the plenum, but the corresponding free volume was not great enough to cause geysering). It is important to point out that geysering did not occur in the annular test program because the annular gap (fig. 9) was open to a large upper plenum, and that the pressure release upon boiling was only a small fraction of the hydrostatic head.

The pressure drop across the test section was measured by using an inverted U-tube manometer. The manometer was connected to the pressure taps located on the brass adapters by epoxy cement. An inverted U-tube manometer was used because it was observed that some of the vapor entering the manometer (which was initially filled with liquid) condensed thus preventing any readings until a sufficient amount of vapor entered the line to cause a permanent (for that run) liquid vapor interface to appear. This would result in a pressure drop reading smaller than the true value. Inversion of the manometer insured a liquid vapor interface being present. A plastic bulb (see fig. 7) was attached to the top of the inverted U and a bubble could be forced in the line prior to each test run. The actual pressure drop was measured by recording the relative height of the liquid in the two columns.

Power was supplied to the test section, PH1, and PH2 by three 220 volt variacs. The power could be regulated from zero to maximum power as desired.

The inner wall temperature in the test section were measured by two thermocouples located 1/16 inch from the .394 inch center hole. Temperatures were measured by a Triplett digital voltmeter. A thermocouple was also inserted in PH2 for purposes of observing when steady state conditions had been reached at a particular power input. All thermocouples were copper-constant and connected to a common ice bath.

B.2 EXPERIMENTAL PROCEDURE AND BRIEF DISCUSSION OF ERRORS

A liquid flow rate was first set and the power to PH2 turned on to a low enough value to just create slug flow bubbles. PH1 was then turned on to adjust the inlet liquid temperature to the plenumb and the system was allowed to come to steady state conditions (usually taking about 15 minutes). The subcooling discussed previously did not effect the test results because once steady state conditions had been reached the amount of vapor entering the plenum from line 3 was sufficient to insure that the liquid flowing into the test section was at the saturation temperature of Freon (i.e., the saturated vapor moving upwards heated the falling liquid in line 3 so that by the time it arrived at the test section it was at the saturation temperature). Hence saturated liquid existed primarily in lines 3 and 4.

Power to the test section was increased in steps until a point was reached at which it appeared that no steady state temperature wxisted for that power setting. Such a point was taken to be the CHF point for the particular flow rates existing at that time. It immediately became apparent that CHF was a rather indeterminate quantity since there was no well defined power input to the test section at which the wall temperature suddenly began to rise. This can be seen to be a consequence of the size of the copper block. When dry patches are formed heat is conducted away from these hot patches essentially cooling the potential CHF location by conduction. The result is that a much slower wall temperature rise at CHF is noted. Then the CHF point becomes indeterminate and a condition known as "slow burnout" results. This appeared to have been the case here since at no time was the wall temperature rise sudden at CHF. This has the effect of increasing the width of the scatter bands for the CHF value. This accounts for the greatest error in recording data. However, upon repeating the procedure three times for identical flow conditions it was found that the CHF values were within 5 to 10 percent of each other, and this was taken to be the error in the recorded CHF values (neglecting instrumentation reading errors).

Once CHF had been reached and recorded for the initial inlet conditions, the power to the test section was reduced by 10% and the voltage to PH2

increased by 10 volts to provide a new inlet superficial vapor velocity to the test section. The liquid flow rate out PH2 (measured by FM2) was kept constant and the above procedure repeated until the inlet conditions to the test section were such as to cause flooding in line 4 (i.e., a set of runs were made with different inlet vapor velocities to the test section). Once this limit had been reached for a given liquid rate out PH2, a new superficial liquid velocity out PH2 was chosen and the above mentioned procedure repeated.

Since void fraction was determined from the pressure drop across the test section (using equ. 26), it was necessary to record the height difference, h, at CHF. This at first presented somewhat of a problem because large oscillations of the liquid in the two columns of the manometer made visual recording of height differences impossible. A number of photographs were taken of the liquid in the column at CHF to record an instantaneous h. The result showed that while the liquid exhibited significant oscillations, the relative height of the liquid in the two columns remained nearly constant (for each set of initial conditions), never deviating by more than 10%. By simply taking the average of the relative heights recorded for a number of photographs, an error of no more than 10% from the average measured values resulted in any single reading (the error was, in most cases lower).

In addition to errors in detecting CHF and recording pressure drop, heat losses from the test section and PH2 were estimated at being no more than 10%. This was shown by removing all liquid from the loop and then turning on the power to the test section to achieve the same temperature that had been recorded at CHF. Also FM1 and FM2 were capable of readings to within 1%. A small amount of throttling of V4 was sufficient to damp out flow oscillations.

Once nucleate boiling began in PH2 and the test section, the natural tendency of the liquid entering the plenum from line 1 was to flow out through line 2 because of the pressure increase of the plenum relative to lines 3 and 4. Hence a certain amount of throttling of VI was necessary in order to force the required amount of liquid out of PH2. If the pump is turned off there still exists a natural circulation of liquid in lines 3 and 4 such that the mass flow rate of vapor ejected into the plenum equals

the liquid flow rate entering line 3.

Fig. B below shows a close-up drawing of the test section and preheater arrangement in which it is seen that there is an initial inlet vapor flow rate, j_{g2}, to the test section. A force balance was performed on the control volume of the test section to arrive at equations similar to eqs. 25 through 28 for the average void fraction.

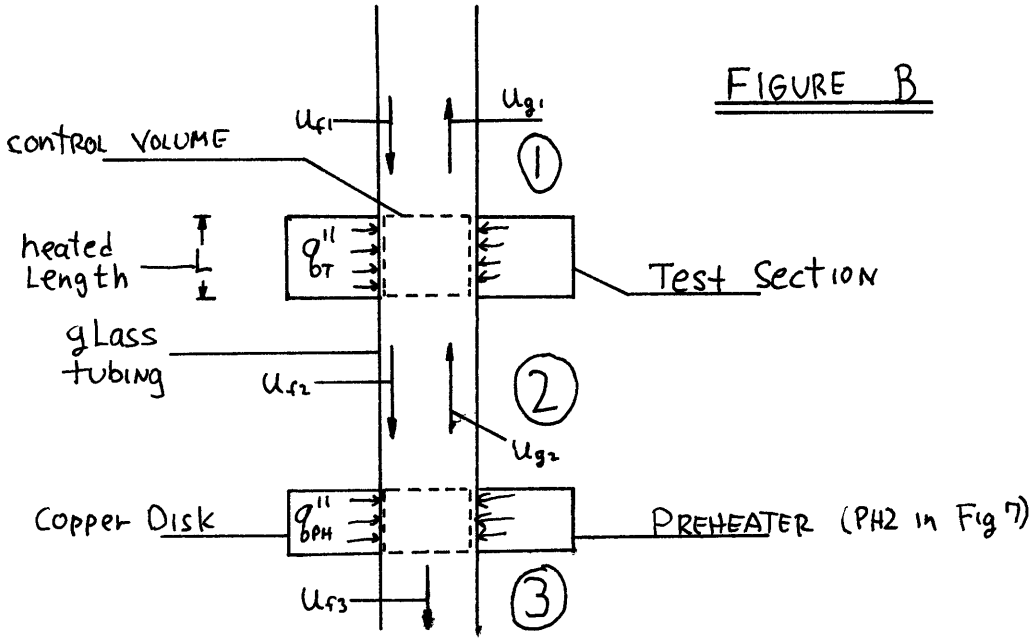

FIGURE B

The major results of the data taken in this program have been mentioned in the body of this report, notably fig. 4.

References

1. Wallis, G.B., One-dimensional Two-phase Flow, McGraw-Hill Book Co., New York, 1969.

2. Zuber, N., Staub, F.W., Bijwaard, G., and Kroeger, P.G., "Steady state and Transient Void Fraction in Two-Phase Flow Systems - Final Report for the Program of Two-Phase Flow Investigation," General Electric Co., Schenectady, New York, Report No. GEAP-5417, 1967.

3. Sherwood, T.K., Shipley, G.H., and Holloway, F.A.L., "Flooding Velocities in Packed Columns," Ind. Eng. Chem., Vol. 30, 1938, pp. 765-769.

4. Hewitt, G.F., and Hall-Taylor, N.S., Annular Two-Phase Flow, Pergamon Press, New York, 1970.

5. Dukler, A.E., "Fluid Mechanics and Heat Transfer in Vertical Falling-Film Systems," Chemical Engineering Progress Symposium Series, Vol. 56, No. 30, 1959, pp. 1-10.

6. Schumann, W.A., "Burnout Heat Flux in Vertical Tubes, Closed at the Bottom, Open to a Pool of Liquid," SM Thesis, Dept. of Mechanical Engineering, MIT, June 1960.

7. Griffith, P., Schumann, W.A., and Neustal, A.D., "Flooding and Burnout in Closed End Vertical Tubes," Paper No. 5, Two-Phase Flow Symposium, Institute of Mechanical Engineers, London, 1962.

8. Shires, G.L., Pickering, A.R., and Blacker, P.T., "Film Cooling of Vertical Fuel Rods," AEEW-R 343, 1964.

9. Sakhuja, R.K., "Flooding Constraint in Wickless Heat Pipes," Thermo Electron Corporation, Waltham, Mass., 1973.

10. Zuber, N., and Findlay, J.A., "Average Volumetric Concentration in Two-phase Flow Systems," ASME Journal of Heat Transfer, Vol. 87, 1965, pp. 453-468.

11. Griffith, P., "Prediction of Low Quality Boiling Voids," ASME Paper No. 63-HT-20, 1963.

12. Janssen, E., Levy, S., and Kervinen, J.A., "Investigations of Burnout in an Internally Heated Annulus Cooled by Water at 600 to 1450 psia," ASME Paper No. 63-WA-149, 1963.

13. Lienhard, J.H., and Keeling, K.B., "An Induced-Convection Effect Upon the Peak-Boiling Heat Flux," Journal of Heat Transfer, Trans. ASME, Series C, Vol. 92, No. 1, Feb. 1970, pp. 1-5.

14. Becker, K.M., and Hernborg, G., "Measurements of Burnout Conditions for Flow of Boiling Water in a Vertical Annulus," ASME Paper No. 63-HT-25, 1963.

15. Tong, L.S., Boiling Heat Transfer and Two-Phase Flow, John Wiley & Sons Inc., New York, 1965.

16. Zuber, N., "Two Phase Flow Stability in Rod Bundles," Invited summary for symposium session on Two-Phase Flow and Heat Transfer in Rod Bundles. ASME Winter Annual Meeting, November 18, 1969.

17. Crowley, J.D., and Bergles, A.E., "Fluid-to-Fluid Modeling of the Hydrodynamic Stability of Flow in Boiling Channels," ASME Paper No. 70-HT-28, 1970.

18. Cermak, J.O., et. al., "The Departure From Nucleate Boiling in Rod Bundles During Pressure Blowdown," ASME Paper No. 70-HT-12, 1970.

19. Gouse, S.W., Jr., "Void Fraction Measurement," MIT Engineering Projects Laboratory Report No. DSR 8734-2, 1964.

20. Wallis, G.B., "The Influence of Liquid Viscosity on Flooding in a Vertical Tube," General Electric Co., Schenectady, New York., Report No. 62. GL-132, 1962.

21. Lienhard, J.H., and Dhir, V.K., "Hydrodynamic Prediction of Peak Pool-Boiling Heat Fluxes from Finite Bodies," ASME Paper No. 72-WA/HT-10, 1972.

22. Costello, C.P., and Adams, J.M., "The Interrelation of Geometry, Orientation, and Acceleration in the Peak Heat Flux Problem," Mechanical Engineering Department Report, University of Washington, Seattle, Wash., 1963.

23. Griffith, P., "Geysering in Liquid-Filled Lines," ASME Paper No. 62-HT-39, 1962.

24. Zuber, N., "Hydrodynamic Aspects of Boiling Heat Transfer," AEC Report No. AECU-4439, 1959.

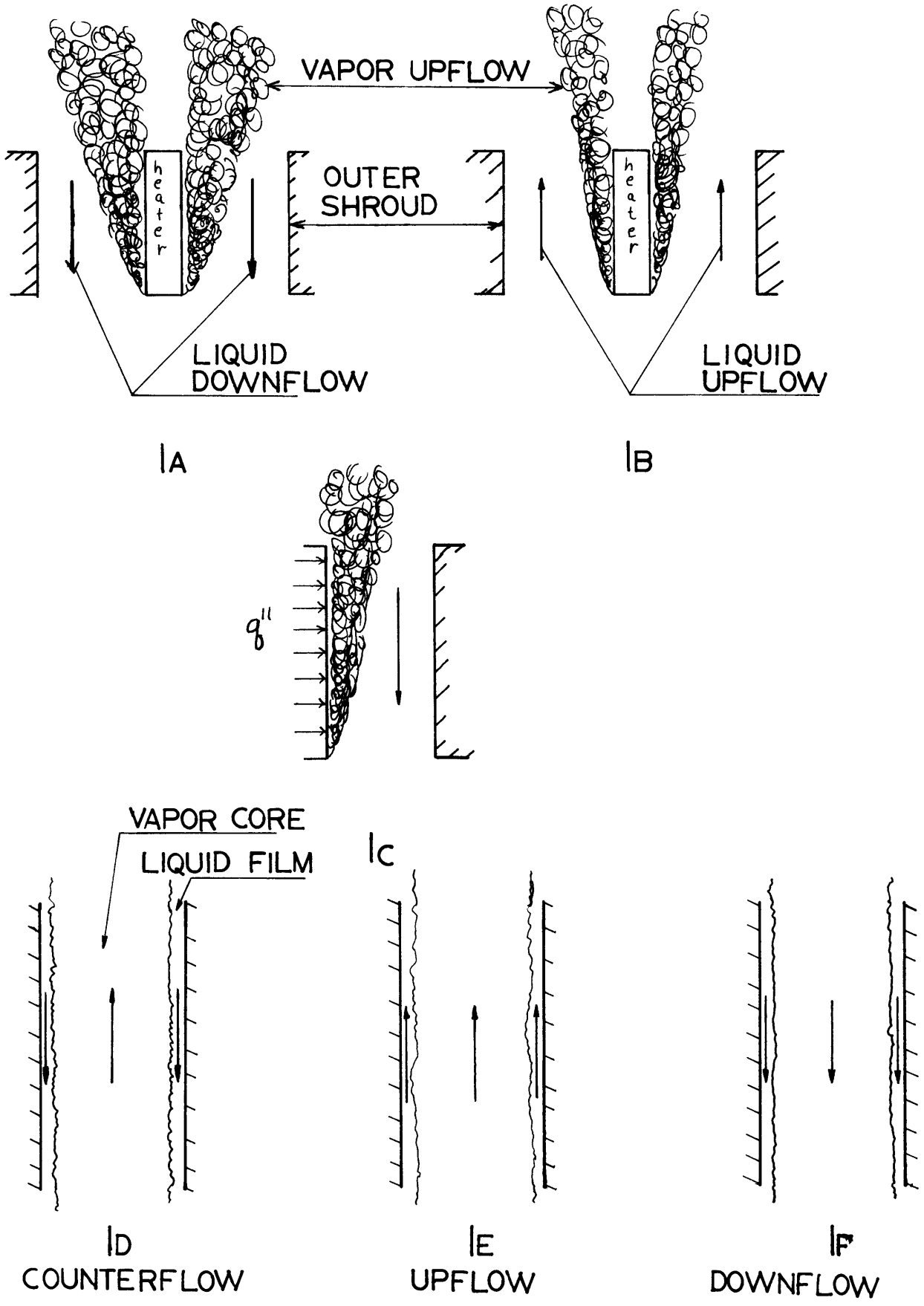

Figure 1. Two-phase flow patterns in an annulus and round tube vertically oriented.

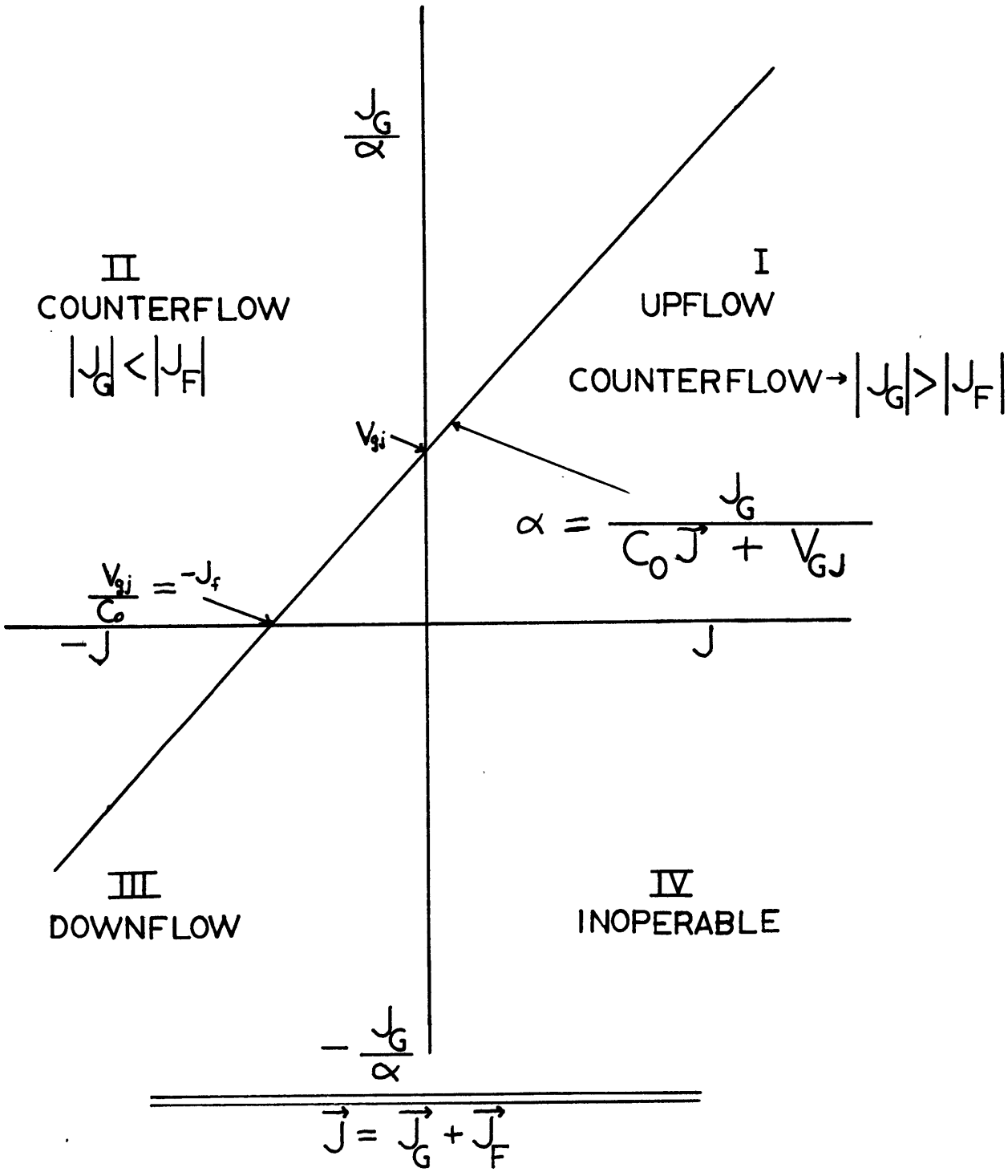

FIGURE 2. Operational regions in two-phase flow.(2).

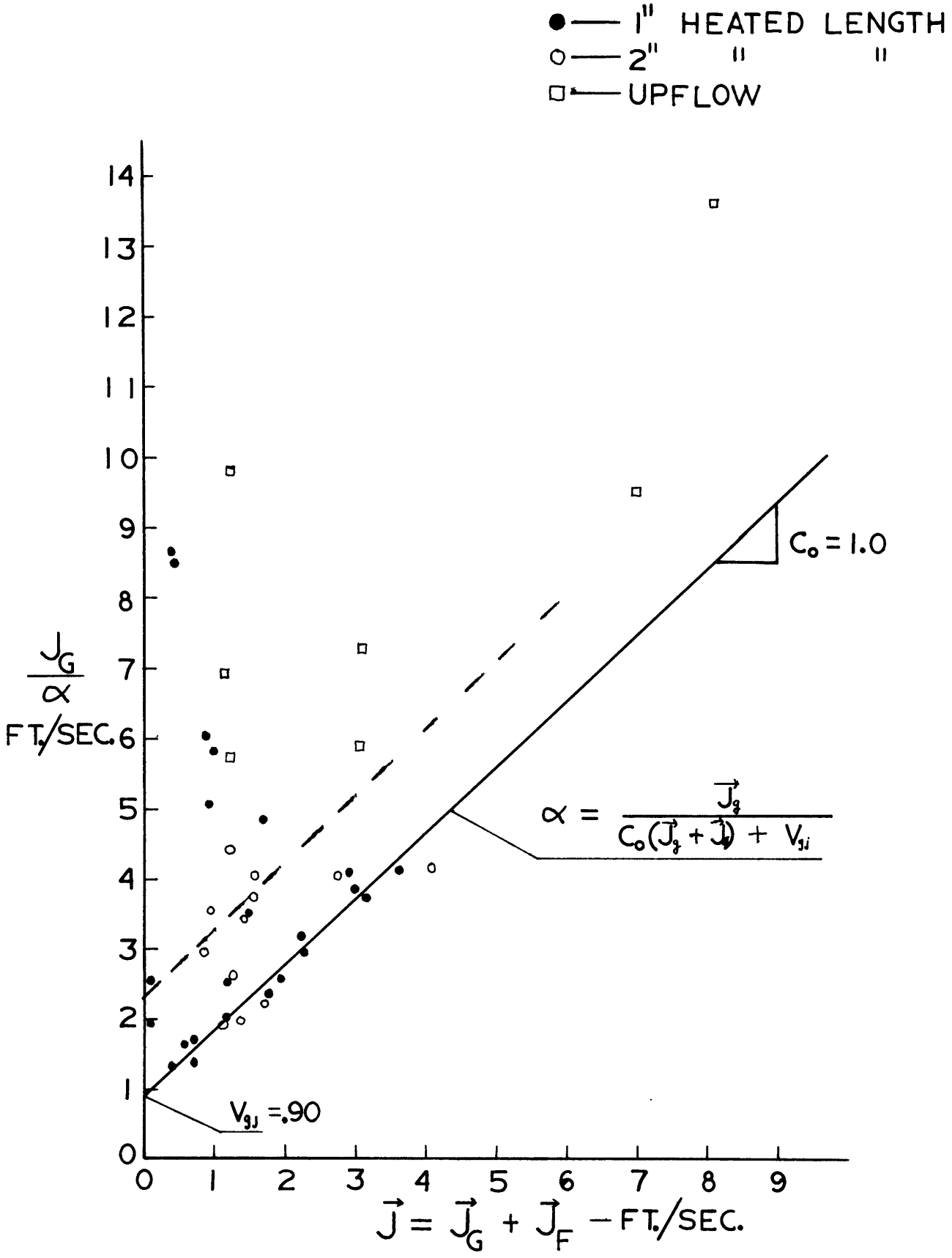

Figure 3. The velocity-flux plane assuming equilibrium flow.

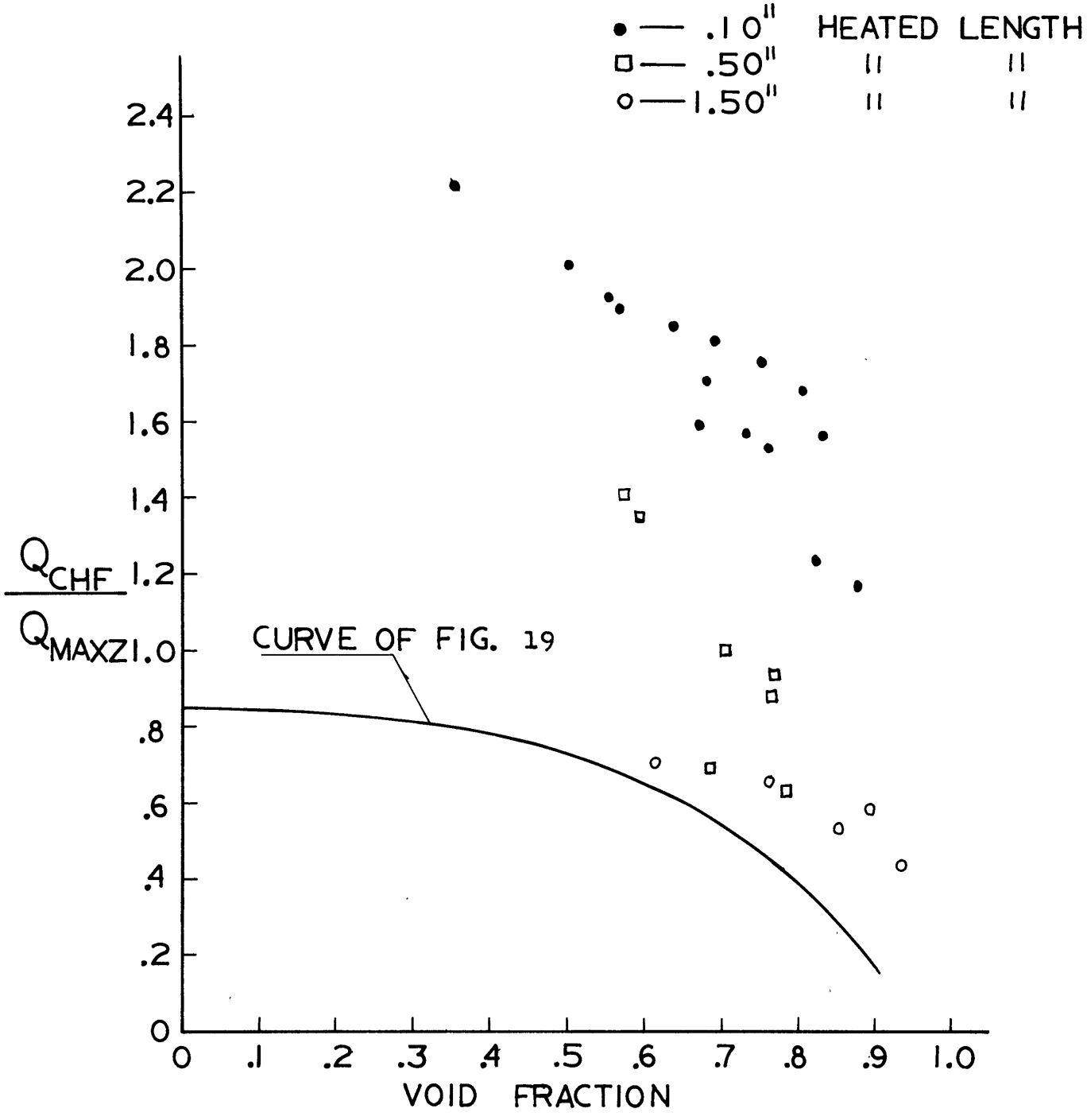

Figure 4. The relation between CHF inside a vertical round tube and a vertical annulus for fluid near saturation (Freon 113).

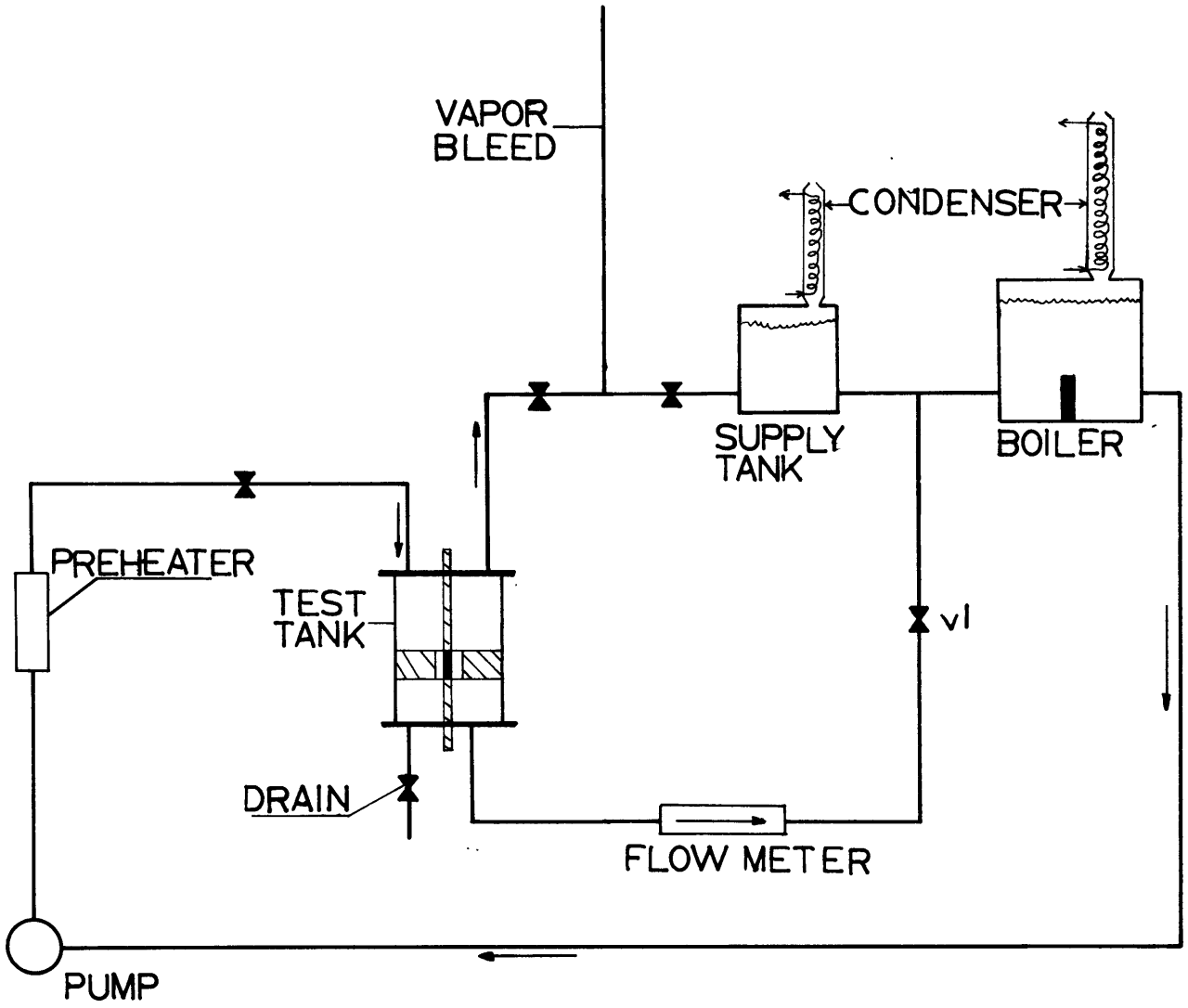

Figure 5. SCHEMATIC OF COUNTERFLOW LOOP

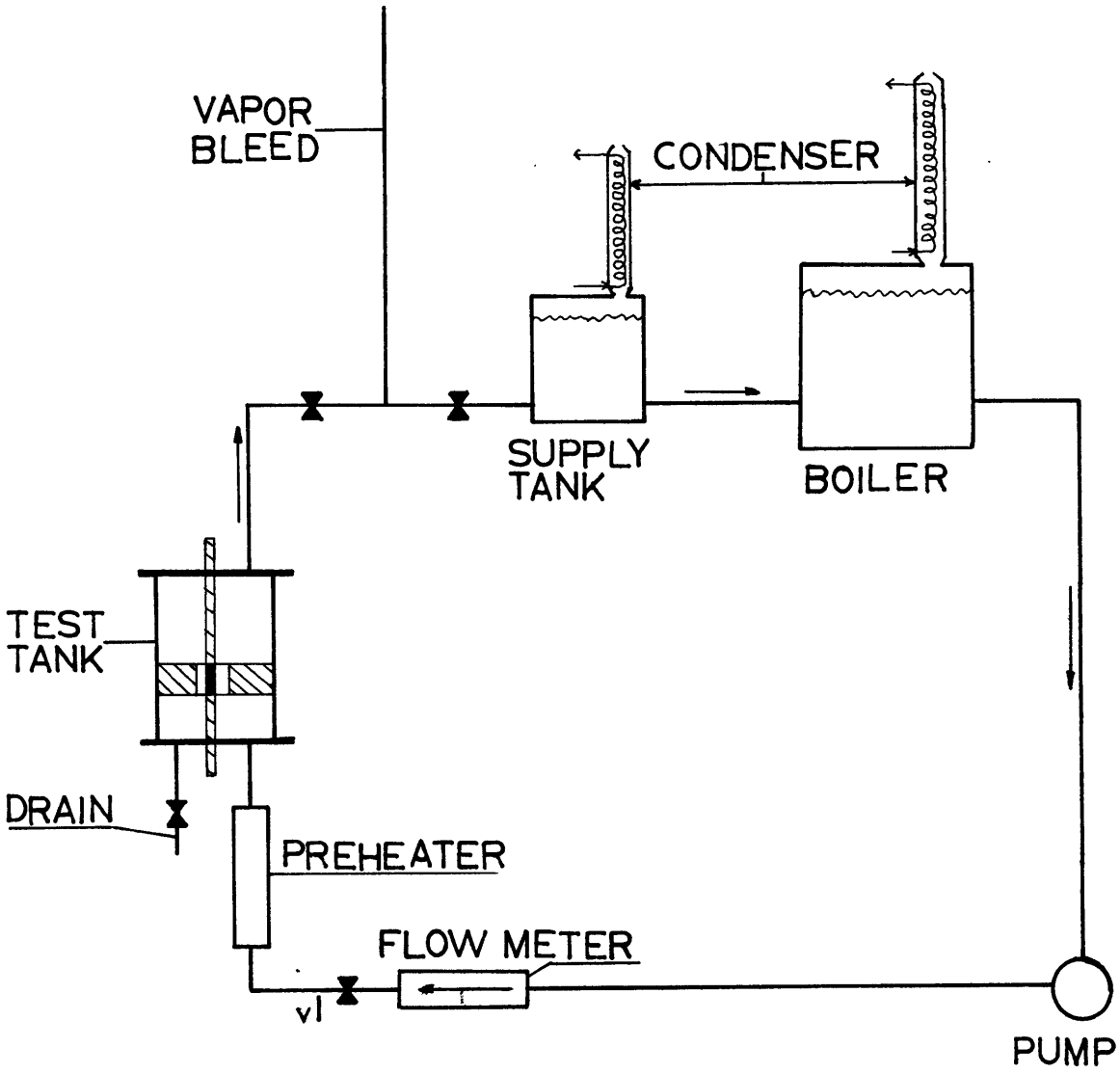

Figure 6. SCHEMATIC OF UPFLOW LOOP

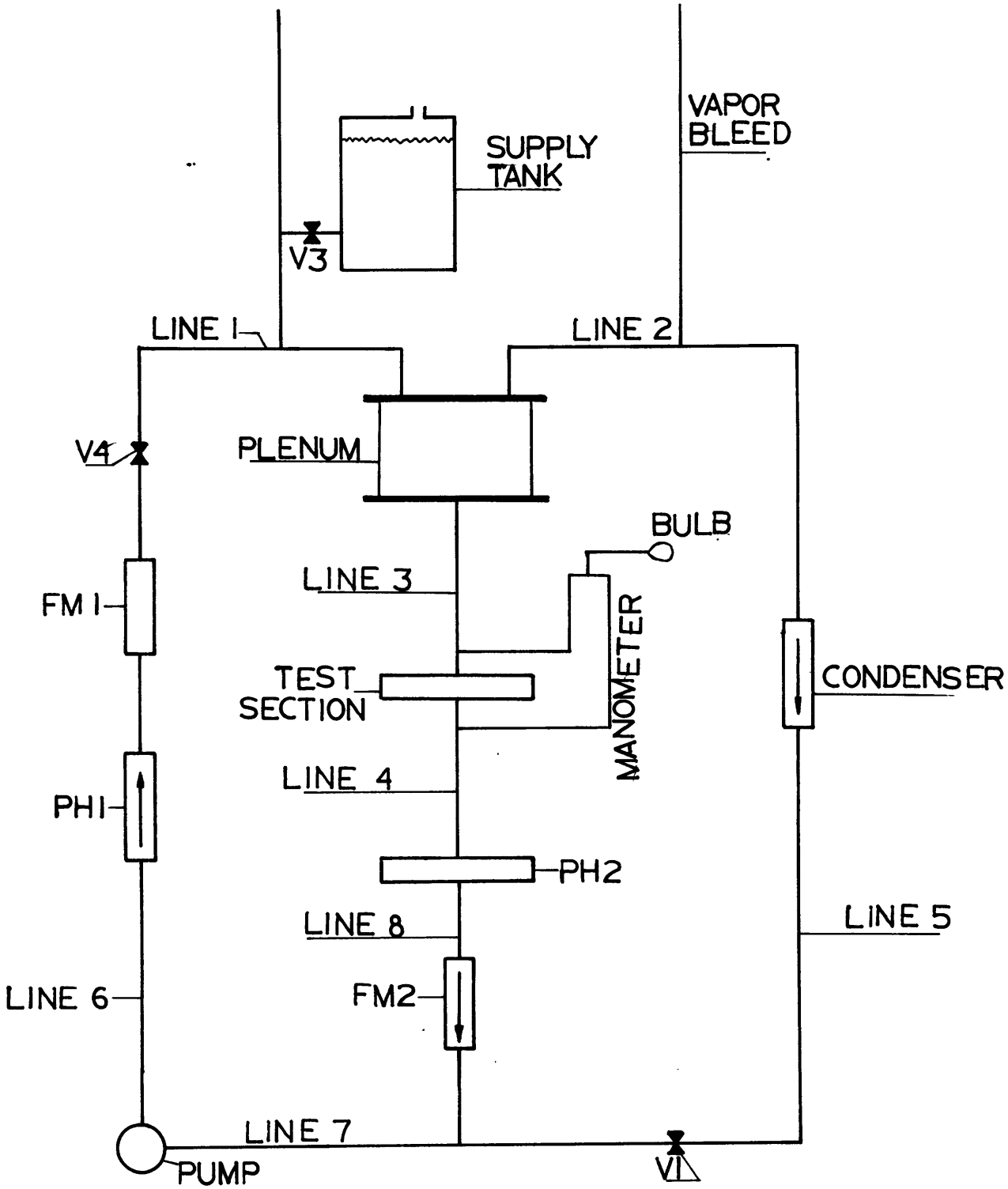

Figure 7. SCHEMATIC OF DUCT FLOW LOOP

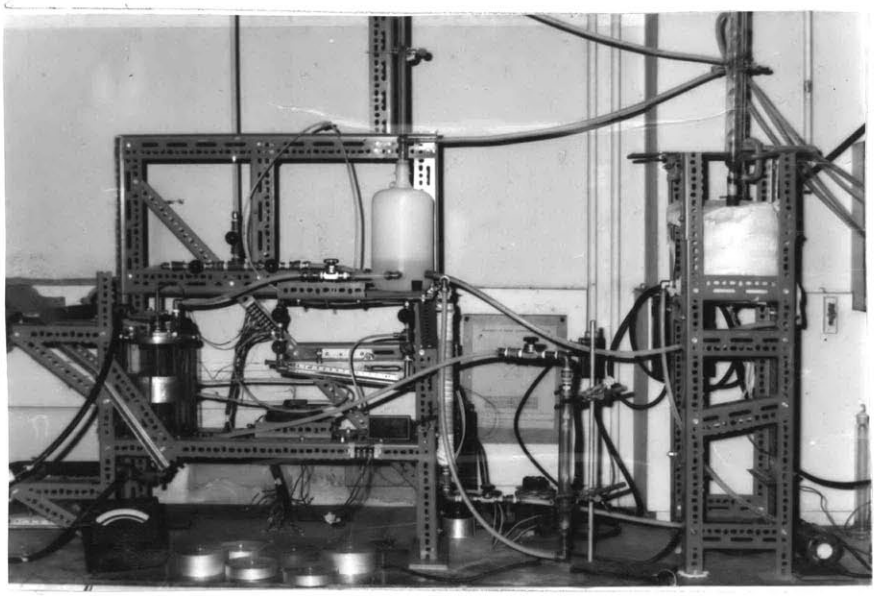

Figure 8a. Photograph of entire apparatus.

Figure 8b. Photograph of test section and test tank.

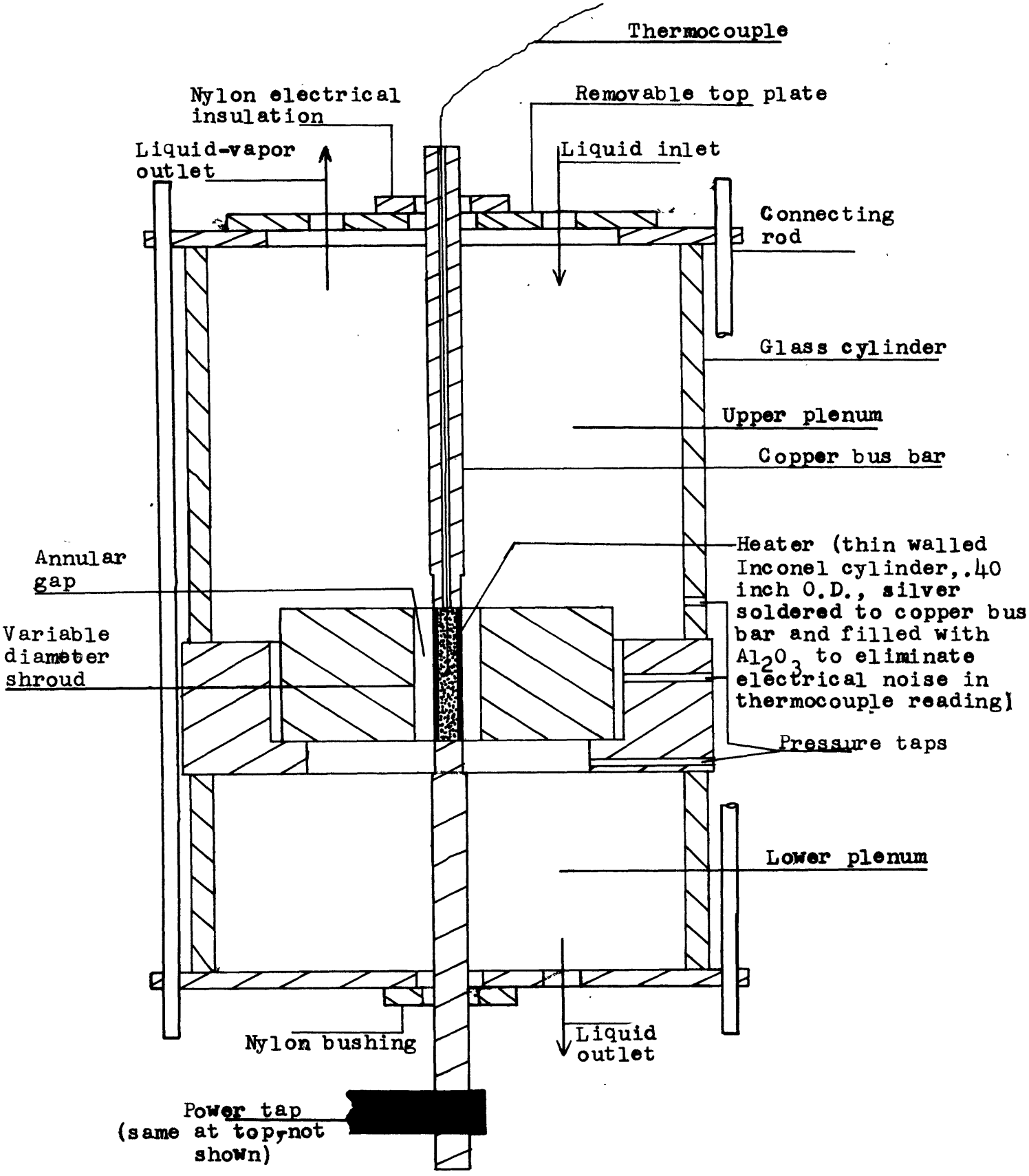

Figure 9. Schematic of test section.

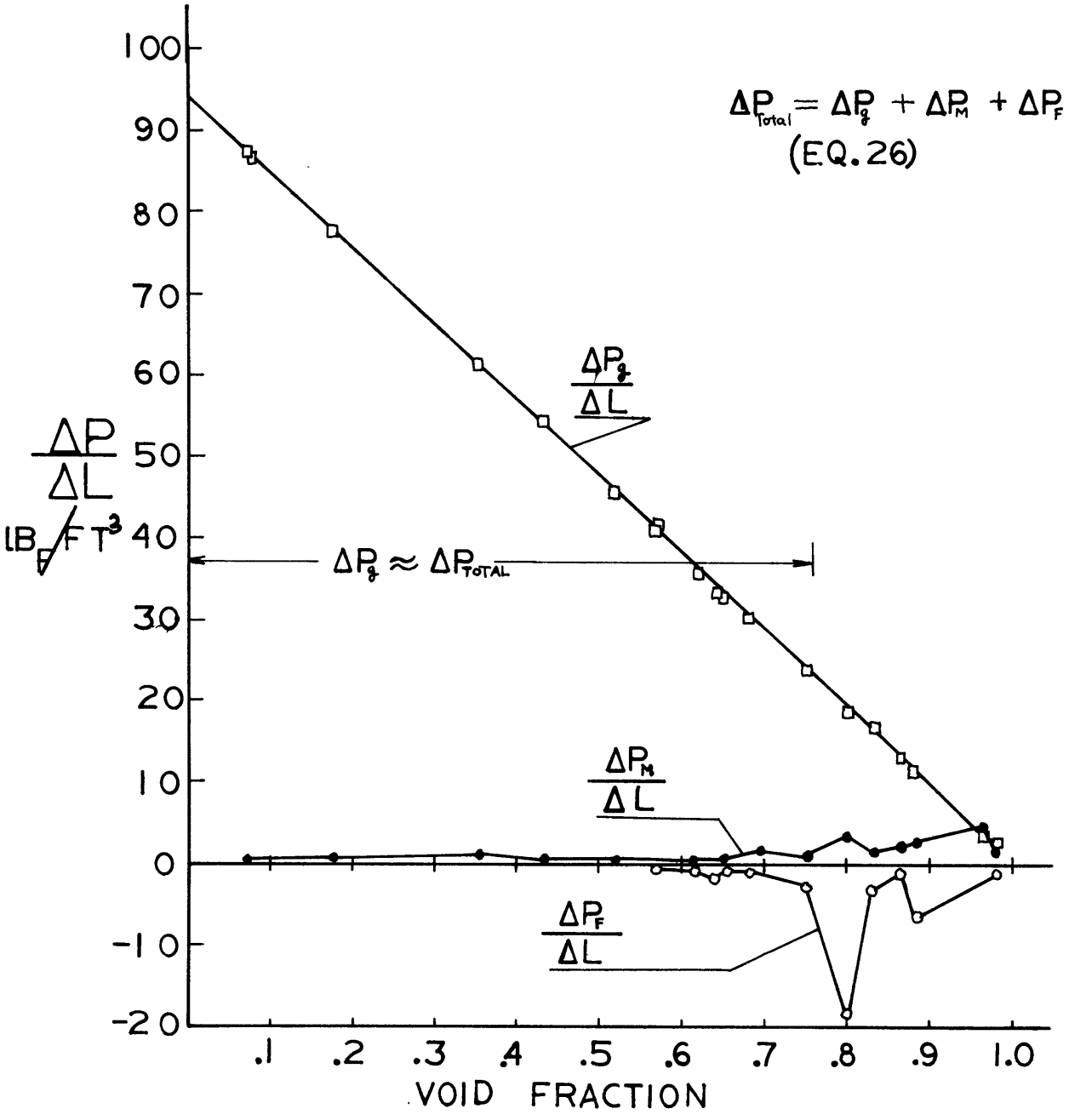

Figure 10. The relative magnitude of the components of eq. 26 with increasing void fraction in counterflow.

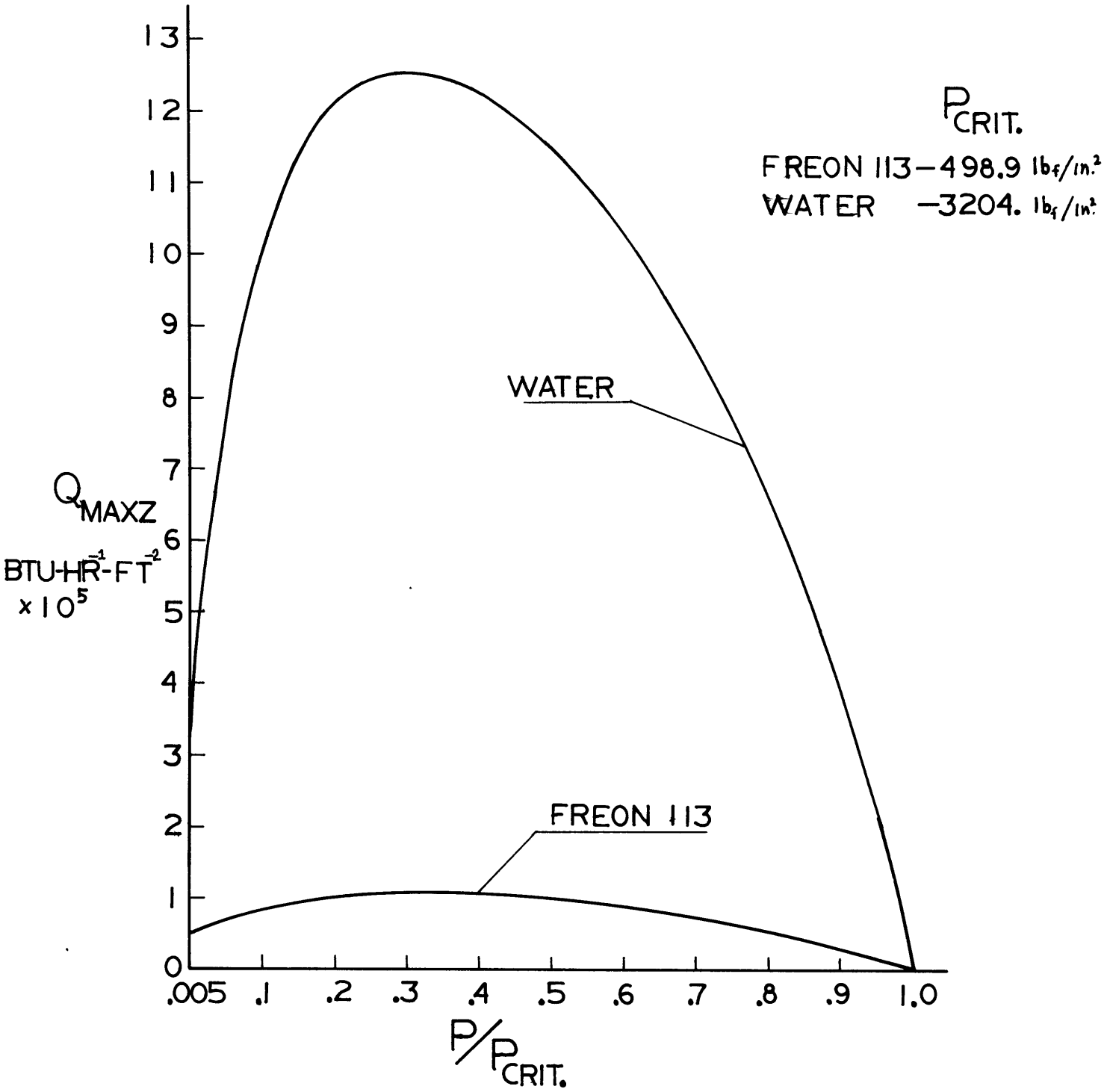

Figure 11. Variation of pool boiling CHF with pressure using Zuber's (24) flat plate prediction.

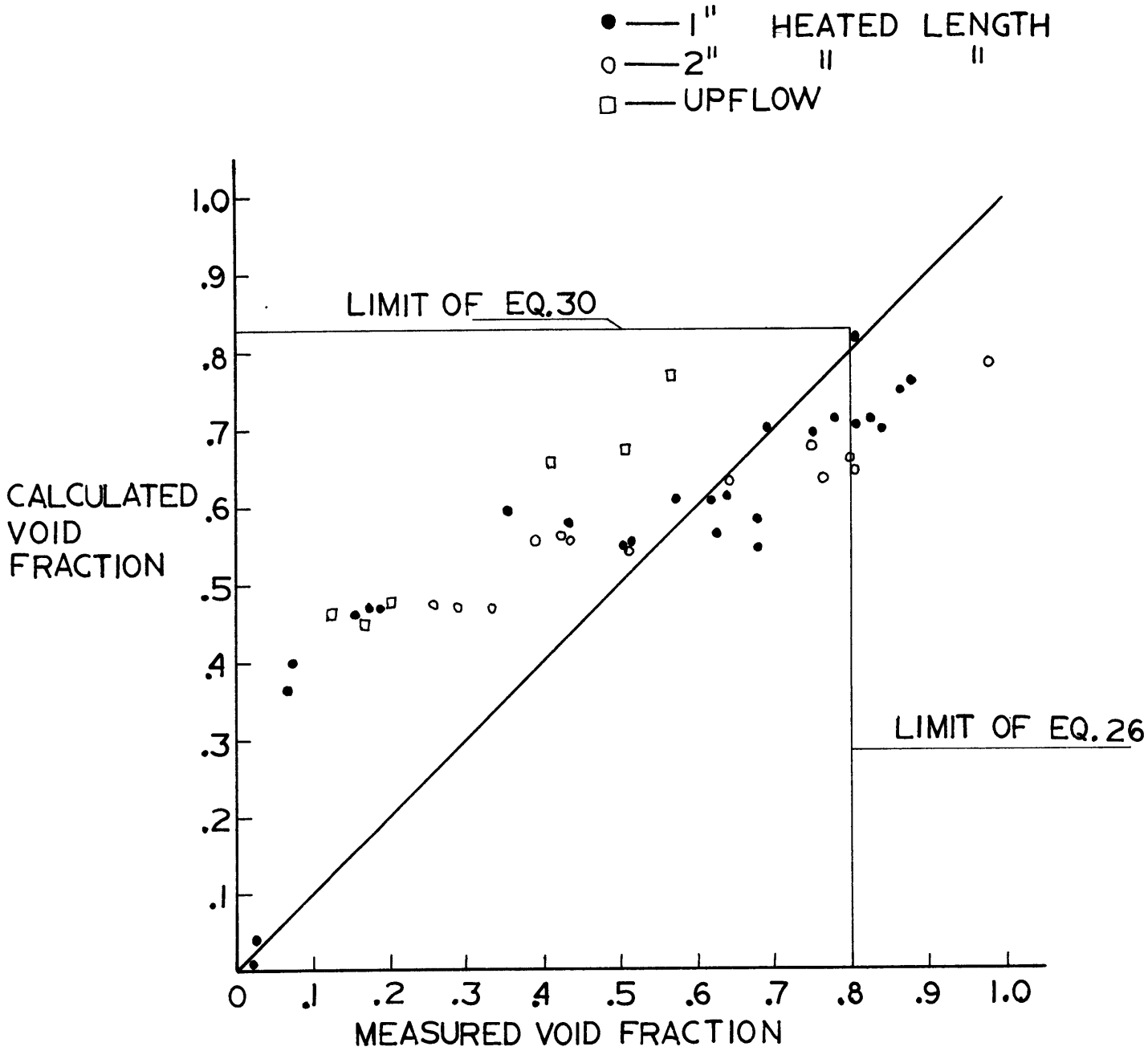

Figure 12. Void obtained from pressure drop data (eq.26) vs. void fraction predicted from the Drift Flux Model assuming equilibrium countercurrent flow.

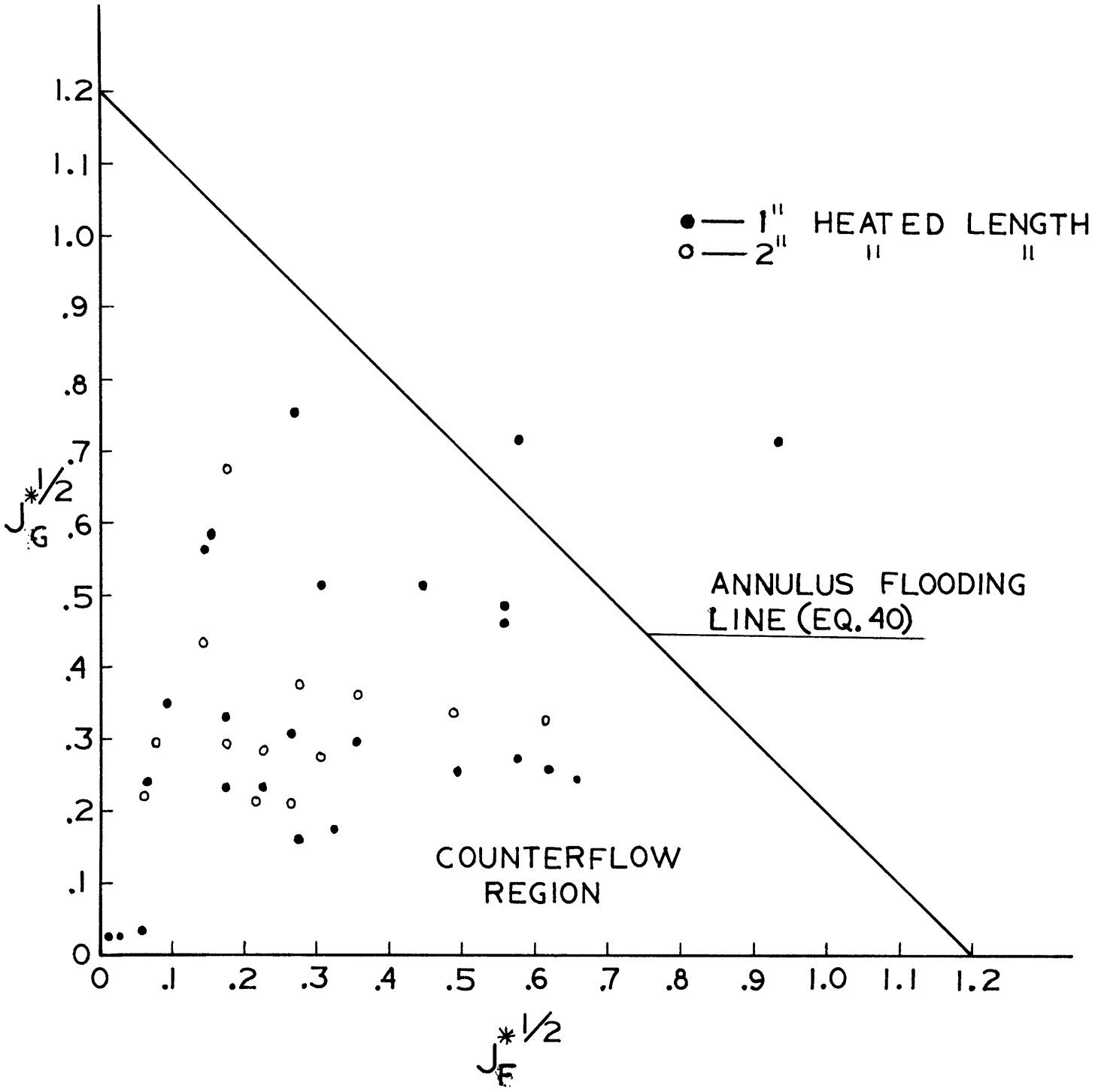

Figure 13. The relation of data obtained to flooding in a vertical annulus.

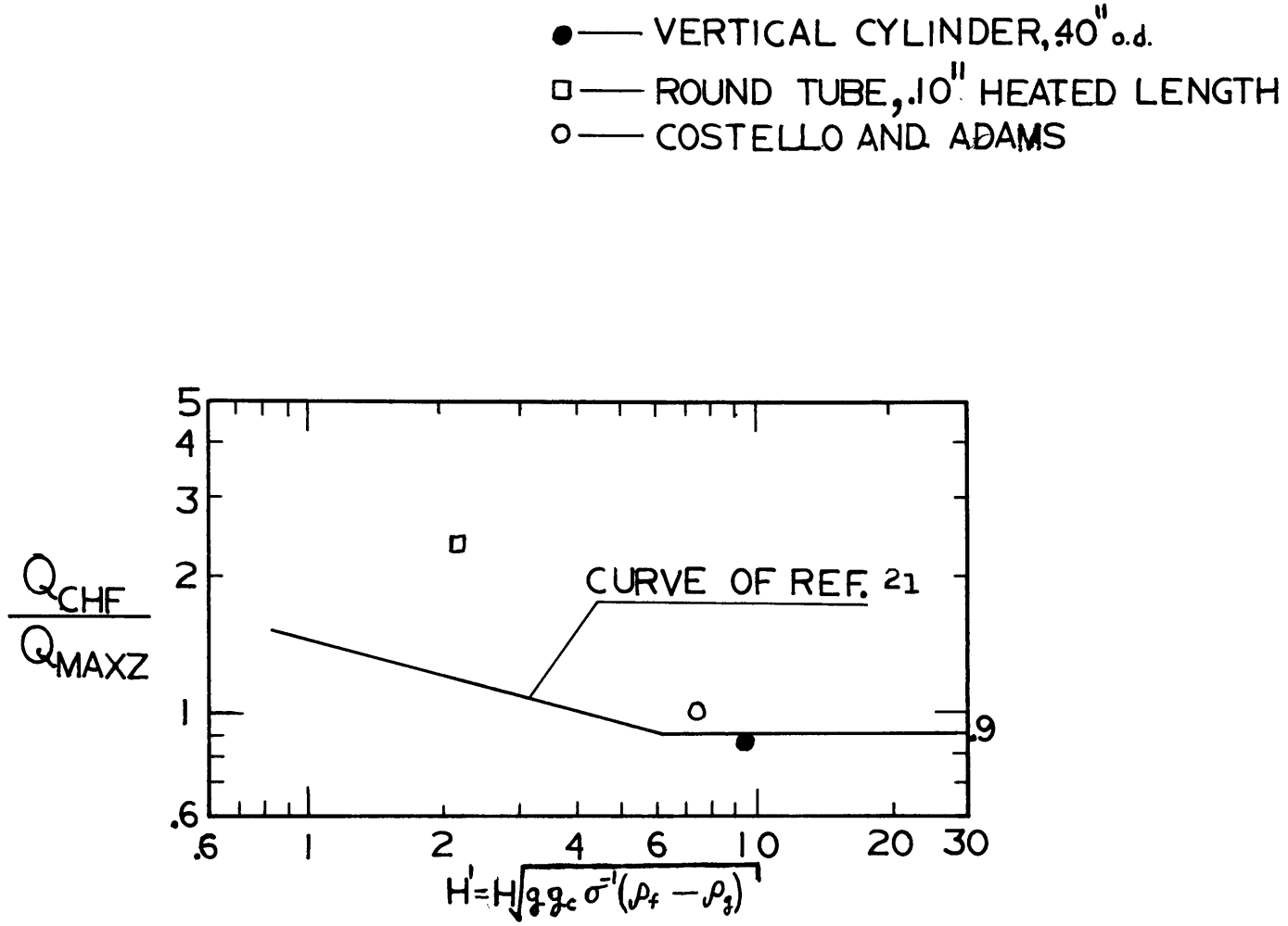

Figure 14. Effect of heater size on CHF where the line is taken from Lienhard (21) and the three points included are from this study. For $H' > 6$, CHF is independent of heater size in pool boiling.

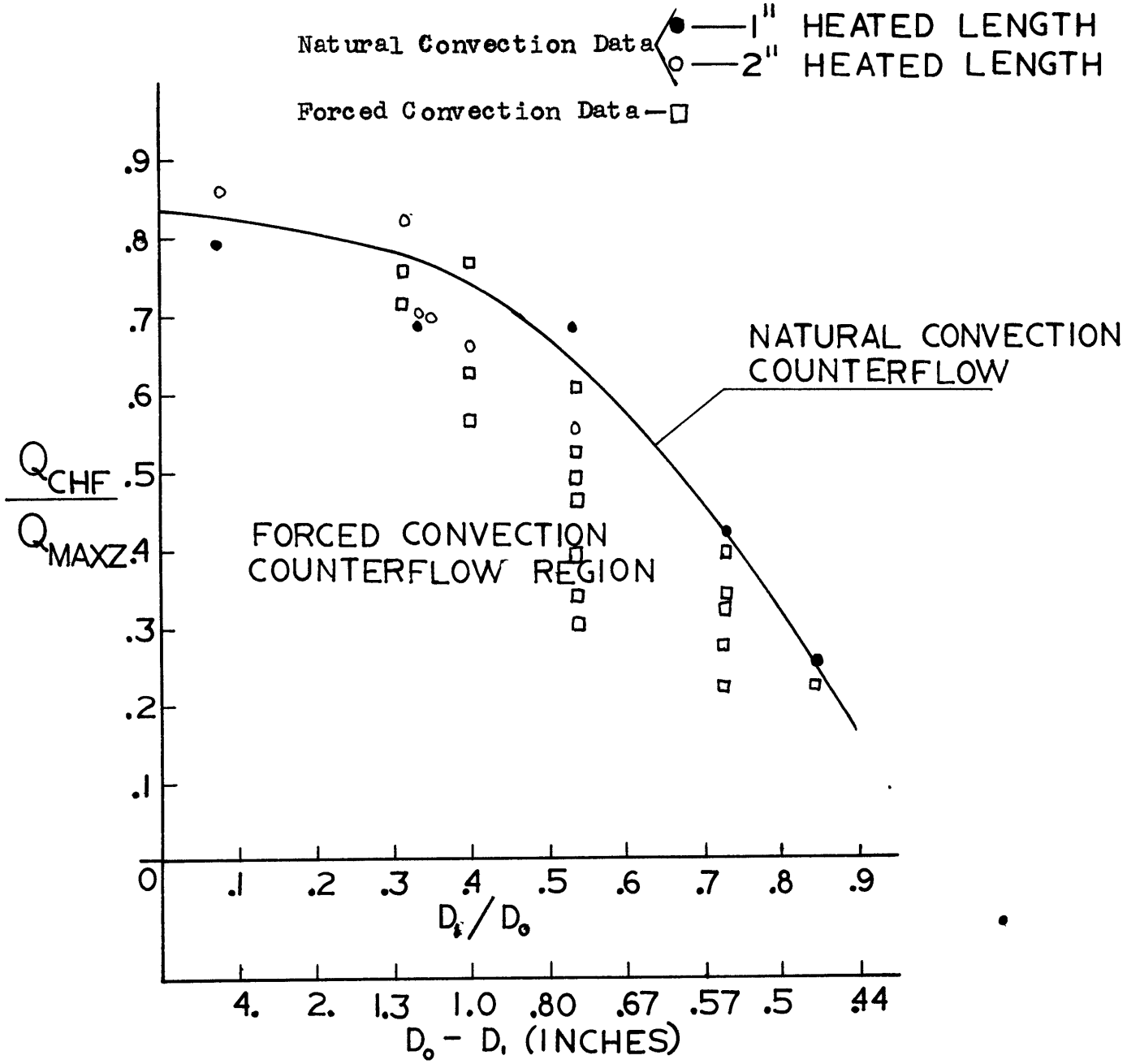

Figure 15. The effect of varying the outer shroud diameter on CHF.

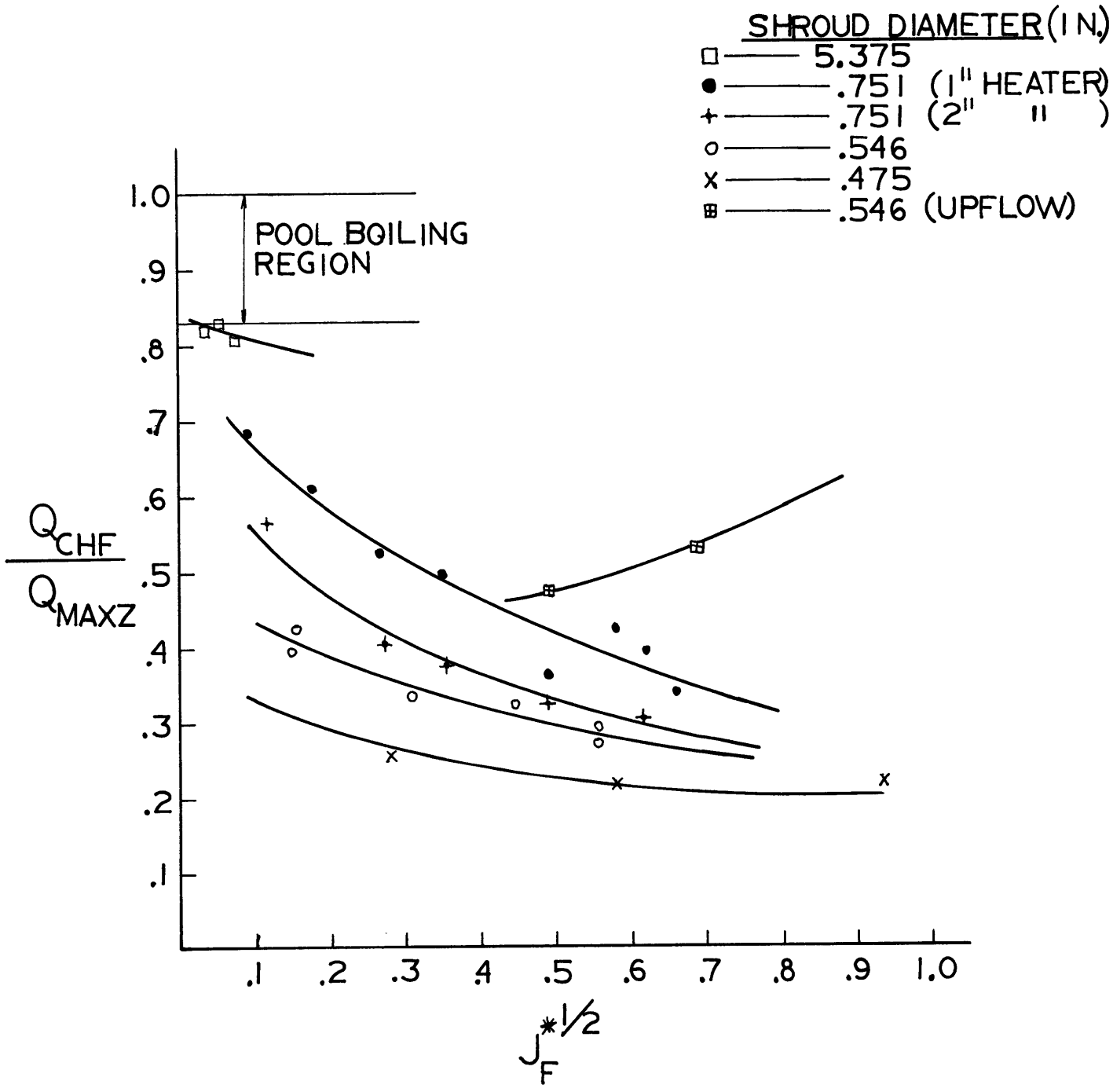

Figure 16. The effect of liquid velocity on CHF for constant outer shroud diameters in equilibrium flow.

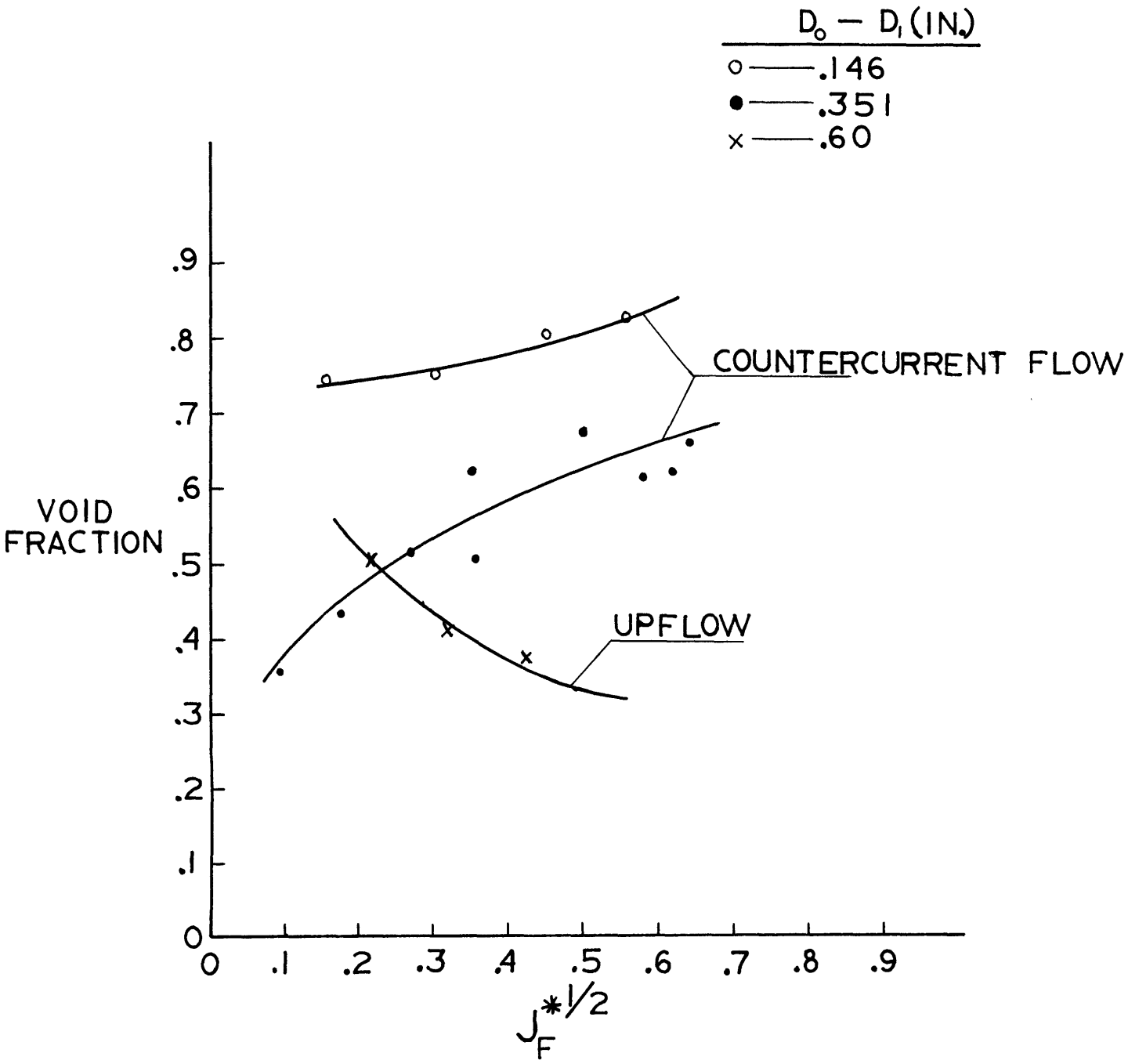

Figure 17. Effect of increasing liquid velocity on void fraction in upflow and countercurrent flow at saturation conditions.

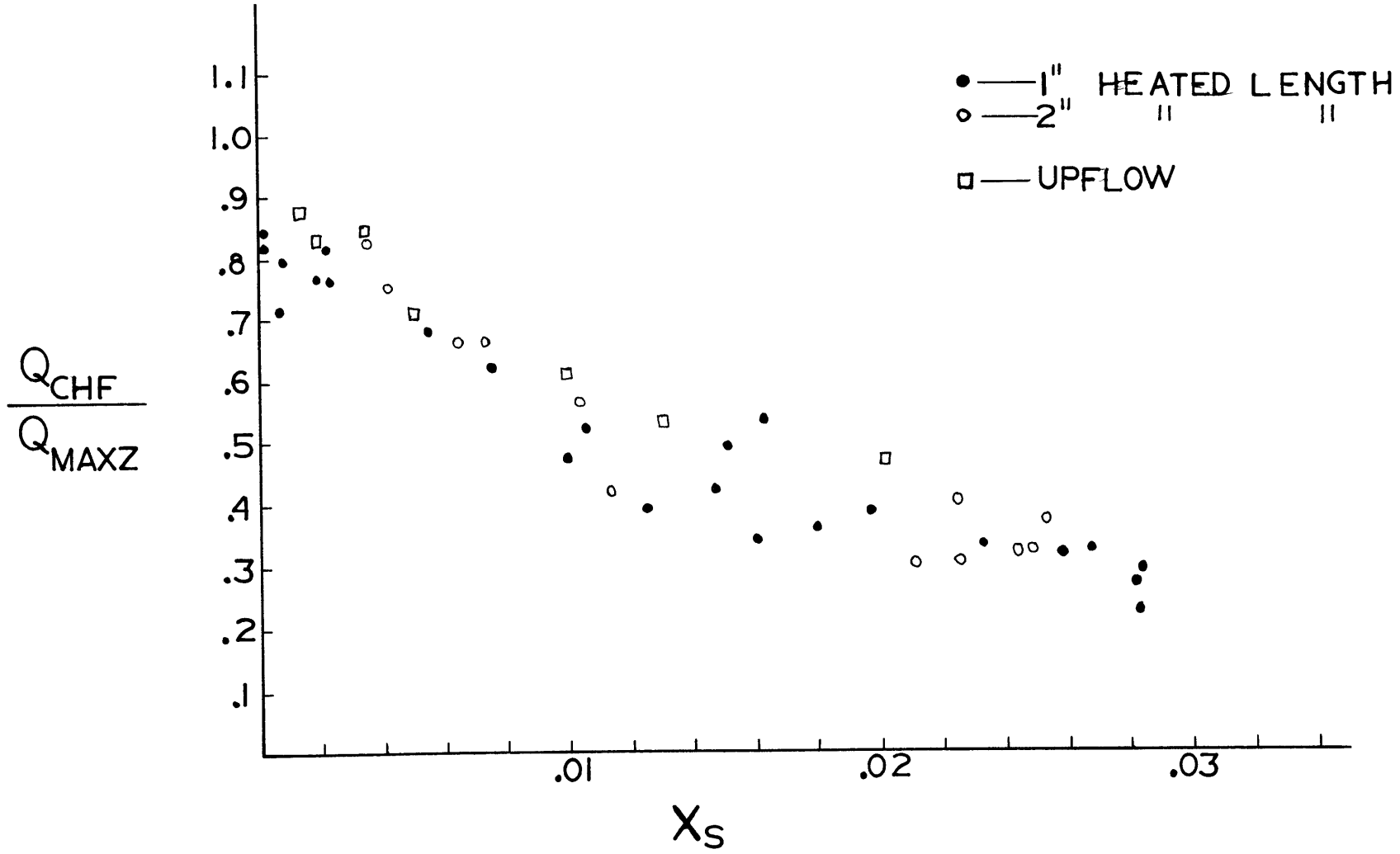

Figure 18. The relation between counterflow CHF (and upflow CHF) and the "in place" quality (eq. 42).

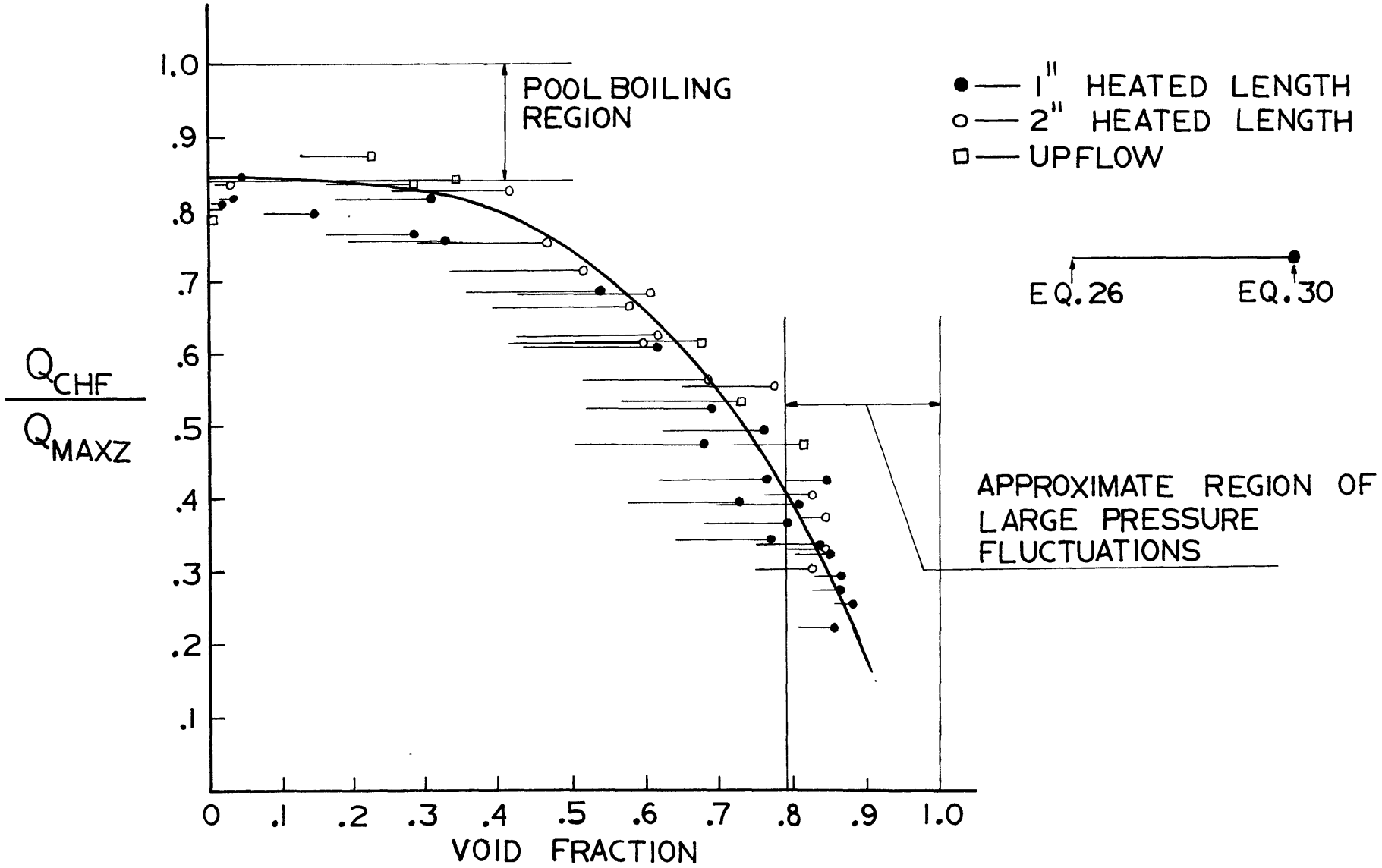

Figure 19. The relation between counterflow CHF, void fraction, and pool boiling from a vertical surface.